IEEE Access
Multidisciplinary ⋮ Rapid Review ⋮ Open Access Journal

Received March 6, 2020, accepted March 21, 2020, date of publication March 25, 2020, date of current version April 7, 2020.

Digital Object Identifier 10.1109/ACCESS.2020.2983328

Effective Capacity Based Power Allocation for the Coexistence of an Integrated Radar and Communication System and a Commercial Communication System

YUNFENG LIU[1], ZHIQING WEI[1], (Member, IEEE), CHENG YAN[2], ZHIYONG FENG[1], (Senior Member, IEEE), AND GORDON L. STÜBER[3], (Fellow, IEEE)

[1]Key Laboratory of Universal Wireless Communications, Ministry of Education, Wireless Technology Innovation Institute (WTI), Beijing University of Posts and Telecommunications, Beijing 100876, China
[2]North China Institute of Computing Technology, Beijing 100083, China
[3]School of Electrical and Computer Engineering, Georgia Institute of Technology, Atlanta, GA 30332, USA

Corresponding author: Zhiyong Feng (fengzy@bupt.edu.cn)

This work was supported by the National Natural Science Foundation of China under Grant 61631003.

ABSTRACT Considerable interest has been shown in the coexistence between airborne radar and commercial communication systems in recent years. In particular, the integrated radar and communication system (IRCS) is promising for the airborne platforms like Unmanned Air Vehicles (UAVs). However, due to fast varying channels caused by high mobility, it is a great challenge for the fusion center to collect detection information within a given delay threshold through the air-to-ground (A2G) communication. Based on slowly varying components of the channel, i.e, target spectrum, power spectral densities of the signal dependent clutters, path loss and shadow fading, this paper considers the problem of power minimization for an IRCS and a base station (BS) coexisting in the same frequency band. The latency bound, latency violation probability (LVP), and channel capacity for the A2G communication to the fusion center are considered based on the effective capacity (EC) theory. The detection performance for radar and the rate requirement of BS user are also taken into account. The power allocation problem is non-convex and formulated to a monotonic optimization problem. Afterward, an efficient heuristic scheduling algorithm with acceptable computational complexity is proposed to solve the formulated problem. Then, the robust power allocation with channel estimation error is considered. Simulation results demonstrate the effectiveness of the proposed heuristic algorithm from the perspectives of the total transmit power, EC, and LVP of the IRCS.

INDEX TERMS Integrated radar and communications, conditional mutual information, latency violation probability, effective capacity.

I. INTRODUCTION

In the past, communications and radar have typically been developed in isolation. However, with the spectral congestion concerns caused by the dramatic rise of commercial wireless communications, considerable interest exists in the coexistence between airborne radar and commercial communication systems in recent years. In the coexistence situation, the airborne radar and commercial communications systems treat one another as interferers, and some knowledge is shared between systems in order to effectively mitigate interference relative to one another [1]–[3].

Moreover, for many platforms, especially airborne ones like manned combat aircrafts or Unmanned Air Vehicles (UAVs) [4], and intelligent transportation systems [5], [6], the payload available for airborne/vehicular communications and radar is limited. Thus, there is a growing interest of electromagnetic radio frequency convergence for the operation of both systems in these platforms, which is named integrated radar and communication system (IRCS). An IRCS has advantages in reducing the system size, weight, and power consumption, and mitigating electromagnetic interference,

The associate editor coordinating the review of this manuscript and approving it for publication was Muhammad Khandaker.

since radar and communication can share the antenna, signal processing hardware and the frequency band [7]. In an IRCS, it is crucial to exploit an integrated signal simultaneously performing the radar and communications functions to improve the spectrum efficiency.

The problem of coexistence of radar and commercial communication systems has been investigated in the literature. A cooperative scheme for the spectral coexistence of a multiple-input-multiple-output (MIMO) communication system and a matrix completion based collocated MIMO radar is proposed [8]. The radar transmit precoder, the radar subsampling scheme, and the communication transmit covariance matrix are jointly designed in order to maximize the radar signal-to-interference-plus-noise ratio (SINR), while guaranteeing specified communication rate and power constraints. A novel power minimization beamforming is proposed in [9]–[11] to enable the coexistence between MIMO radar and downlink multiuser multi-input single-output communication system. The multiuser interference is explored to improve the communication performance and reduce the transmit power of the radar. The research in [12] states that minimizing the MMSE (minimum mean square error) in estimating the target impulse response is equivalent to maximizing the conditional mutual information (MI). In terms of sharing the same frequency band, multicarrier systems are considered to be among the best candidates for both radar sensing and communications applications [13]. Motivated by the recent interest in multicarrier radar system and the theory of MI, several multicarrier-based radar power allocation algorithms in spectral sharing environments are presented [14]–[16]. The power allocation for radar is designed with the knowledge provided by the communication systems [14]. It maximizes the MI with interference constraints that maintain the capacity of the communication channels above a threshold and a power constraint on the radar. As an extension, three criteria differ in the way the communication signals scattered off the target are considered, i.e., as useful energy, as interference, or ignored at the radar receiver [15]. Further, based on the three criteria, the uncertainty of the target spectra bounded by known upper and lower bounds are considered to minimize the worst-case radar transmitted power [2]. The situation that multiple radars coexist with a communication system is studied in [17]. The problem of non-cooperative game theoretic power allocation for distributed multiple-radar architectures in a spectrum sharing environment is constructed.

There has also been considerable work on the power allocation for an IRCS in the literature. Paul *et al.* provide a point of departure for future researchers that will be required to solve the problem of spectral congestion by presenting the applications, topologies, levels of system integration, the current state of the art, and outlines of future systems in [18]. Moreover, a novel joint estimation and information theoretic bound formulation for a receiver that observes communication and radar returns in the same frequency is constructed by Bliss [19] and Chiriyath *et al.* [20]–[22]. The joint performance bound is presented in terms of the uplink communication rate and the estimation rate of the system. An IRCS based on multicarrier is considered in [23]. The integrated signal is used for both detection and communication. With a constraint on the total power, the optimization problem, which simultaneously considers the conditional MI for radar and channel capacity for communications, is devised, and the analytic solution is derived. The designed integrated signal outperforms the fixed signal, i.e., equal power allocation, with lower transmit power. Similarly, the power allocation for the IRCS is designed to minimize the total radiated power, while satisfying the specified requirements of target parameter estimation and data information rate [3]. As an extension, a wireless powered IRCS is proposed [24]. An energy minimization problem is formulated subject to constraints on the radar and communication performances. The energy beamforming and power allocation are jointly considered to minimize energy consumption.

Much work has been directed to the performance of the coexistence of airborne radars and base stations (BSs) from the perspective of MI and channel capacity [2], [15]. Besides, the power allocation for the airborne IRCS has been studied [3], [23]. To the best of our knowledge, these two scenarios are separately studied in the previous works. Therefore, the coexistence of the airborne IRCS and BS are considered in this paper, which is extended from the results in [2], [3], [23]. The detection information obtained by the airborne platform should be transmitted to the fusion center by air-to-ground (A2G) communication [25], [26]. As the target is moving, the detection information is time-sensitive. Thus, for the communication performance of the airborne IRCS, except for the channel capacity, the latency requirement should also be considered. Besides, latency violation probability (LVP) characterizes the tail behavior of the random latency, which also deserves concern.

In this paper, with the goal to minimize the total transmit power of the IRCS, the power allocation of the IRCS and the BS for each subcarrier is cooperatively designed. The MI requirement for detection and the rate requirement of the BS user are considered. As for the A2G communication performance of the IRCS, the latency bound, LVP, and channel capacity are taken into account. Based on effective capacity (EC) theory, the A2G communication performance is achieved with slowly varying channel information, i.e, target spectrum, power spectral densities (PSDs) of the signal dependent clutters, path loss and shadow fading, instead of instantaneous channel information, which handles the challenge caused by high mobility. The primal power allocation issue is formulated as a monotonic optimization problem, and the optimal result can be obtained through the polyblock outer approximation algorithm in [27]. The computational complexity of the polyblock outer approximation algorithm involved in solving the problem is much more manageable than generic algorithms. However, the complexity is still high and cannot be guaranteed within polynomial time. Then, an efficient heuristic scheduling algorithm with computational complexity of $O\left(200N\log\left(1/\varepsilon_0\right)\right)$ is proposed to solve

the monotonic optimization problem, where ε_0 is the error tolerance of the bisection search algorithm. Besides, the robust power allocation with channel estimation error is considered. Finally, extensive simulation results are provided to verify the superior performance of the heuristic algorithm.

The remainder of this paper is organized as follows. Section II introduces the system model. Then, the power allocation scheme is formulated to a monotonic optimization problem, and a low-complexity heuristic algorithm is proposed in Section III. Afterwards, simulation results are presented to confirm the effectiveness of the designed algorithm in Section IV. Finally, Section V concludes the paper.

II. SYSTEM MODEL

A. SCENARIO

In this section, a coexistence scenario illustrated in Fig. 1 is considered, where a UAV employing the IRCS and a commercial BS operate with the same carrier frequency. The IRCS can perform radar and A2G communication functions simultaneously. In the scenario, the IRCS transmits a signal to the target and fusion center. It is assumed that the radar antenna is directional and steered toward the target. The BS simultaneously transmits the data to BS user by broadcasting signals throughout the space. Without loss of generality, a single UAV and one BS is considered in the scenario. However, the model and derivations can easily be extended to a distributed multiple-UAV system. If the IRCS of each UAV uses different frequencies [28], there is no interference between the UAVs, and the model in this paper can be applied directly. Otherwise, the interference between the UAVs [17] can be used to update the model. Thus, the model can be applied to the scenario where multiple UAVs employing the IRCS coexist with a communication system in the same frequency band, which is similar to the scenarios in [17], [29].

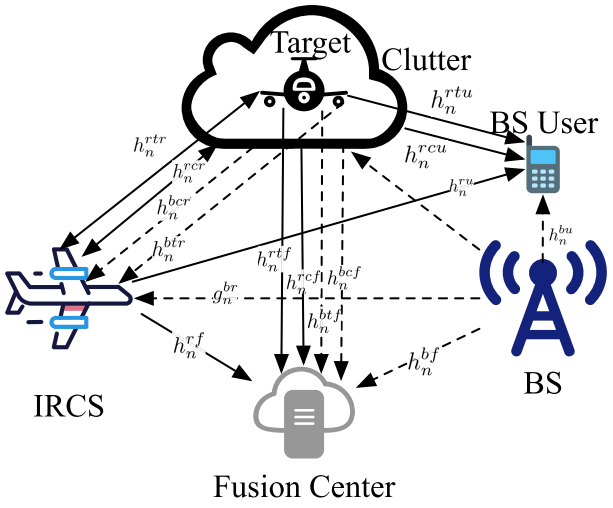

FIGURE 1. Illustration of the system model.

B. CHANNEL MODEL

The received signal at the IRCS contains: the echo radar signal scattered from the target and clutter, the echo BS signal scattered from the target and clutter, and the BS signal from the direct path. Assuming that there are N subcarriers in the system, the corresponding path losses of the channels for the nth subcarrier are g_n^{rtr}, g_n^{rcr}, g_n^{btr}, g_n^{bcr}, and g_n^{br}, which are modeled as

$$\begin{aligned} g_n^{rtr} &= g_n^{rcr} = \frac{G_t G_r \lambda_n^2}{(4\pi)^3 d_{rt}^4} \\ g_n^{btr} &= g_n^{bcr} = \frac{G_s G_r \lambda_n^2}{(4\pi)^3 d_{bt}^2 d_{rt}^2} \\ g_n^{br} &= \frac{G_s^2 \lambda_n^2}{(4\pi)^2 d_{br}^2} \end{aligned} \tag{1}$$

where G_t and G_r are the main-lobe transmitting and receiving antenna gain of the IRCS, respectively, and G_s is the antenna gain of the BS and the side-lobe transmitting/receiving antenna gain of the IRCS. λ_n is the wavelength of the nth subcarrier. d_{rt}, d_{bt}, and d_{br} denote the distances between the radar and the target, between the BS and the target, and between the BS and the radar, respectively.

The channel power gain of the radar-target-radar, radar-clutter-radar, BS-target-radar, and BS-clutter-radar channels are denoted as h_n^{rtr}, h_n^{rcr}, h_n^{btr}, and h_n^{bcr}, respectively. They are given by [2], [30], [31]

$$\begin{aligned} h_n^{rtr} &= \left|H_n^{rtr}\right|^2 g_n^{rtr} \\ h_n^{rcr} &= P_n^{rcr} g_n^{rcr} \\ h_n^{btr} &= \left|H_n^{btr}\right|^2 g_n^{btr} \\ h_n^{bcr} &= P_n^{bcr} g_n^{bcr}, \end{aligned} \tag{2}$$

where $\left|H_n^{rtr}\right|$ is the target spectrum for the radar-target-radar path, and P_n^{rcr} denotes the PSDs of the signal-dependent clutters for the radar-clutter-radar path [1], [2]. $\left|H_n^{btr}\right|$ and P_n^{bcr} have similar meanings. Thus, the SINR of the radar signal is

$$\Gamma_n^r = \frac{p_n^r h_n^{rtr}}{p_n^r h_n^{rcr} + p_n^{BS}\left(h_n^{btr} + h_n^{bcr} + g_n^{br}\right) + \delta_n^2}, \tag{3}$$

where p_n^r and p_n^{BS} are the transmit power of the IRCS and BS for the nth subcarrier, respectively, and δ_n^2 is the power of the additive white Gaussian noise.

The conditional MI enables one to evaluate the estimation accuracy of the extended target impulse response, which can be utilized as an appropriate metric for radar target characterization. Previously, the analytical expression of conditional MI has already been derived in [23]. Thus, the conditioned MI for the IRCS can be written as [2], [12], [23]

$$MI = \frac{B}{2}\sum_{n=0}^{N-1} \ln\left(1 + \Gamma_n^r\right), \tag{4}$$

where B is the bandwidth of each subcarrier.

Similarly, the received signal at the fusion center contains: the radar signal from the direct path, the echo radar signal scattered from the target and clutter, the echo BS signal scattered from the target and clutter, and the BS signal from

the direct path. The corresponding path losses of the channels for the nth subcarrier are g_n^{rf},g_n^{rtf},g_n^{rcf}, g_n^{btf}, g_n^{bcf}, and g_n^{bf}, which are denoted as

$$\begin{aligned} g_n^{rf} &= \frac{G_s^2\lambda_n^2}{(4\pi)^2 d_{rf}^2}, \\ g_n^{rtf} &= g_n^{rcf} = \frac{G_t G_s \lambda_n^2}{(4\pi)^3 d_{rt}^2 d_{ft}^2}, \\ g_n^{btf} &= g_n^{bcf} = \frac{G_s^2\lambda_n^2}{(4\pi)^3 d_{bt}^2 d_{ft}^2}, \\ g_n^{bf} &= \frac{G_s^2\lambda_n^2}{(4\pi)^2 d_{bf}^2}, \end{aligned} \tag{5}$$

where d_{rf}, d_{ft}, and d_{bf} denote the distances between the radar and the fusion center, between the fusion center and the target, and between the BS and the fusion center, respectively. As the fusion center is on the ground, the shadow fading and small-scale fading are taken into account when the latency boundary and LVP requirements the A2G communication are considered. The corresponding channel power gain are

$$\begin{aligned} h_n^{rf} &= g_n^{rf}\beta_n^{rf}\alpha_n^{rf} = \gamma_n^{rf}\alpha_n^{rf} \\ h_n^{rtf} &= \left|H_n^{rtf}\right|^2 g_n^{rtf}\beta_n^{rtf}\alpha_n^{rtf} = \gamma_n^{rtf}\alpha_n^{rtf} \\ h_n^{rcf} &= P_n^{rcf} g_n^{rcf}\beta_n^{rcf}\alpha_n^{rcf} = \gamma_n^{rcf}\alpha_n^{rcf} \\ h_n^{btf} &= \left|H_n^{btf}\right|^2 g_n^{btf}\beta_n^{btf}\alpha_n^{btf} = \gamma_n^{btf}\alpha_n^{btf} \\ h_n^{bcf} &= P_n^{bcf} g_n^{bcf}\beta_n^{bcf}\alpha_n^{bcf} = \gamma_n^{bcf}\alpha_n^{bcf} \\ h_n^{bf} &= g_n^{bf}\beta_n^{bf}\alpha_n^{bf} = \gamma_n^{bf}\alpha_n^{bf}, \end{aligned} \tag{6}$$

where β_n^{rf} and α_n^{rf} account for the corresponding shadow fading and small- scale fading, respectively. β_n^{rtf}, α_n^{rtf}, β_n^{rcf}, α_n^{rcf}, β_n^{btf}, α_n^{btf}, β_n^{bcf}, α_n^{bcf}, β_n^{bf}, and α_n^{bf} have similar meanings. $\left|H_n^{rtf}\right|$ is the target spectrum for the radar-target-fusion center path. P_n^{rcf} denotes the PSDs of the signal-dependent clutters for the radar-clutter-fusion center path. $\left|H_n^{btf}\right|$ and P_n^{bcf} have similar meanings. Thus, the SINR of the fusion center can be given by

$$\Gamma_n^f = \frac{p_n^r\left(h_n^{rf} + h_n^{rtf} + h_n^{rcf}\right)}{p_n^{BS}\left(h_n^{bf} + h_n^{btf} + h_n^{bcf}\right) + \delta_n^2}. \tag{7}$$

As mentioned in [32], [33], the latency for the nth subcarrier can be characterized statistically by employing the quality-of-service exponent θ_n, $n = 1, \ldots, N$. Actually, from the EC theory, the EC of the nth subcarrier, denoted by $EC_n(\theta_n)$, represents the maximum supportable arrival data rate for guaranteeing the latency characterized by θ_n [32], and is given by

$$EC_n(\theta_n) = -\frac{1}{\theta_n T}\ln E\left\{e^{-\theta_n TB\ln\left(1+\Gamma_n^f\right)}\right\}. \tag{8}$$

If the arrival data rate of the nth subcarrier, given by $\lambda_{n,0}$, is equal to the EC, i.e., $\lambda_{n,0} = EC_n(\theta_n)$, the LVP of the nth subcarrier is given by [32]

$$P_n\{d_n \geq d_{\max}\} \approx p\left(\lambda_{n,0}\right) e^{-\theta_n\lambda_{n,0}d_{\max}}, \tag{9}$$

where $d_{\max}$ is the latency bound, $p\left(\lambda_{n,0}\right)$ is the probability that the buffer of the nth subcarrier is nonempty in the steady state, which can be approximated by [33], [34]

$$p\left(\lambda_{n,0}\right) \approx \frac{\lambda_{n,0}}{E\left\{B\ln\left(1+\Gamma_n^f\right)\right\}} < 1. \tag{10}$$

In this sense, θ_n provides the exponential decaying rate of the probability that the threshold $d_{\max}$ is exceeded.

As for the BS user, the downlink communication rate is considered. The received signal at the BS user contains: the BS signal, the echo BS signal scattered from the target and clutter, the echo radar signal scattered from the target and clutter, and the radar signal from the direct path. It is assumed that the echo BS signal scattered from the target and clutter is much weaker than that coming through the direct path, and can be ignored for simplicity. The corresponding path losses of the channels for the nth subcarrier are g_n^{bu}, g_n^{rtu}, g_n^{rcu} and g_n^{ru}, which are written as

$$\begin{aligned} g_n^{bu} &= \frac{G_s^2\lambda_n^2}{(4\pi)^2 d_{bu}^2}, \\ g_n^{rtu} &= g_n^{rcu} = \frac{G_t G_s \lambda_n^2}{(4\pi)^3 d_{rt}^2 d_{tu}^2}, \\ g_n^{ru} &= \frac{G_s^2\lambda_n^2}{(4\pi)^2 d_{ru}^2}, \end{aligned} \tag{11}$$

where d_{bu}, d_{tu}, and d_{ru} denote the distance between the BS and the BS user, between the target and the BS user, and between the radar and the BS user, respectively. Assuming that $d_{bt} \gg d_{bu}$ and $d_{br} \gg d_{bu}$, it can be obtained that $d_{tu} \approx d_{bt}$, $d_{ru} \approx d_{br}$, and $g_n^{ru} \approx g_n^{br}$. These approximations are used in the simulations. Since the BS user focuses most on transmission capacity, the small-scale fading is not considered for simplification. The channel power gains of the corresponding channels are given by

$$\begin{aligned} h_n^{bu} &= g_n^{bu}\beta_n^{bu} \\ h_n^{rtu} &= \left|H_n^{rtu}\right|^2 g_n^{rtu}\beta_n^{rtu} \\ h_n^{rcu} &= P_n^{rcu} g_n^{rcu}\beta_n^{rcu} \\ h_n^{ru} &= g_n^{ru}\beta_n^{ru}, \end{aligned} \tag{12}$$

where β_n^{bu}, β_n^{rtu}, β_n^{rcu}, and β_n^{ru} account for the corresponding shadow fading, $\left|H_n^{rtu}\right|$ is the target spectrum for the radar-target-BS user path, and P_n^{rcu} denotes the PSDs of the signal-dependent clutters for the radar-clutter-BS user path. Then, the capacity of the BS user on the nth subcarrier is given by $B\ln\left(1+\Gamma_n^{BS}\right)$, where Γ_n^{BS} is the SINR of the nth subcarrier, and can be written as

$$\Gamma_n^{BS} = \frac{p_n^{BS} h_n^{bu}}{p_n^r\left(h_n^{rtu} + h_n^{rcu} + h_n^{ru}\right) + \delta_n^2}. \tag{13}$$

In the system, time is divided into slots with length T, and L continuous slots form a block. The target spectrum, PSDs of the signal dependent clutters, path loss and shadow fading of all channels are assumed to remain constant during the period of a block since the locations of IRCS, target, and BS user do not change too much. However, considering the high mobility of the IRCS and the target, the small-scale fading components are assumed to be constant during a slot but vary independently from one slot to another.

As the clutter is stable, it is assumed that the clutter responses h_n^{rcr} and h_n^{bcr} can be formed by the radar receiver through previous received signals before the target appears [3], [30]. Similarly, γ_n^{rcf} and γ_n^{bcf} can be obtained by the fusion center, and h_n^{rcu} can be obtained by the BS user. After the target is detected, the radar transmits a reference signal A, and this is used by the radar to estimate h_n^{rtr}, used by the fusion center to observe γ_n^{rf} and γ_n^{rtf}, and used by the BS user to obtain h_n^{rtu} and h_n^{ru}. The BS transmits a reference signal B, and this is used by the radar to estimate h_n^{btr}, used by the fusion center to observe γ_n^{bf} and γ_n^{btf}, and used by the BS user to obtain h_n^{bu} [2], [8], [29]. Moreover, given the location of the IRCS and BS, the fusion center can be aware of the path loss g_n^{br}.

The channel information h_n^{bu}, h_n^{rtu}, h_n^{rcu}, and h_n^{ru} are sent to the BS by the BS user. Then, the IRCS and BS send all channel information to the fusion center. With channel information feedback once per block, the fusion center can be aware of all channels' slowly varying components, i.e, target spectrum, PSDs of the signal dependent clutters, path loss and shadow fading. The statistical characterizations of the small-scale components are known by the fusion center while the exact values of the small-scale fading components during a slot are unknown. Depending on the conditions of the obstacles, the A2G channel has LoS (line-of-sight) or NLoS (non-line-of-sight) characteristics [35], [36]. In this paper, NLoS characteristics, i.e., ergodic Rayleigh small-scale fading, are assumed for the channels to the fusion center. It is assumed that α_n^{rf}, α_n^{rtf}, α_n^{rcf}, α_n^{btf}, α_n^{bcf}, and α_n^{bf} are independent and exponentially distributed with unit mean for all subcarriers. When part of the A2G channels have LoS characteristics, i.e., Rice small-scale fading, a numerical solution can be applied to obtain $F_Z(Z)$ in (61) instead of an analytical solution. The analysis of other parts in this paper stays the same. The shadow fading is a log-normal random variable with a standard deviation ξ. With the channel information collected, the fusion center jointly computes optimal power allocation schemes for both systems and sends each scheme back to the corresponding system [8].

III. ADAPTIVE POWER ALLOCATION ALGORITHM

A. OPTIMAL POWER ALLOCATION ALGORITHM

The aim of our paper is to design the power allocation algorithm for the IRCS and BS to minimize the total transmit power of the IRCS. Considering the predetermined requirements of conditional MI, EC, latency bound, LVP, and BS user data rate, the optimization problem can be formulated as

$$
\begin{aligned}
(\boldsymbol{P1}): \min_{p_n^r, p_n^{BS}, \lambda_{n,0}, \theta_n} & \sum_{n=0}^{N-1} p_n^r && \text{(14a)}\\
& B\ln\left(1+\Gamma_n^{BS}\right) \geq C_n^0 && \text{(14b)}\\
& \frac{B}{2}\sum_{n=0}^{N-1}\ln\left(1+\Gamma_n^r\right) \geq \phi_{MI}^0 && \text{(14c)}\\
& -\frac{1}{\theta_n T}\ln E\left\{e^{-\theta_n TB\ln\left(1+\Gamma_n^f\right)}\right\} = \lambda_{n,0} && \text{(14d)}\\
& \frac{\lambda_{n,0}}{E\left\{B\ln\left(1+\Gamma_n^f\right)\right\}} e^{-\theta_n\lambda_{n,0}d_{\max}} \leq p_0 && \text{(14e)}\\
& \sum_{n=0}^{N-1}\lambda_{n,0} = \lambda_0 && \text{(14f)}\\
& 0 \leq p_n^r \leq p_{n,\max}^r && \text{(14g)}\\
& 0 \leq p_n^{BS} \leq p_{n,\max}^{BS} && \text{(14h)}\\
& \theta_n > 0, && \text{(14i)}
\end{aligned}
$$

where C_n^0 is the minimum required data rate for the downlink BS user on the nth subcarrier, and ϕ_{MI}^0 denotes the specified MI threshold for target characterization performance. $\lambda_{n,0}$ and λ_0 represent the EC on the nth subcarrier and the total EC, respectively. $d_{\max}$ is the latency bound, and p_0 represents the LVP requirement, which are predefined. $p_{n,\max}^r$ and $p_{n,\max}^{BS}$ are the maximum transmit power of the IRCS and BS on the nth subcarrier, respectively. For simplicity, define

$$
\begin{aligned}
f_{1,n}\left(p_n^r, p_n^{BS}\right) &= \ln\left(1+\Gamma_n^{BS}\right),\\
f_{2,n}\left(p_n^r, p_n^{BS}\right) &= \ln\left(1+\Gamma_n^r\right),\\
f_{3,n}\left(p_n^r, p_n^{BS}, \theta_n\right) &= -\frac{1}{\theta_n T}\ln E\left\{e^{-\theta_n TB\ln\left(1+\Gamma_n^f\right)}\right\},\\
f_{4,n}\left(p_n^r, p_n^{BS}, \theta_n, \lambda_{n,0}\right) &= \frac{\lambda_{n,0}}{E\left\{B\ln\left(1+\Gamma_n^f\right)\right\}} e^{-\theta_n\lambda_{n,0}d_{\max}},\\
C_n &= C_n^0/B, \phi_{MI} = 2\phi_{MI}^0/B. \qquad \text{(15)}
\end{aligned}
$$

However, problem P1 is non-convex and it is difficult to obtain the optimal result. The following lemma is presented, proven in Appendix A, as a preliminary to simplify problem P1.

Lemma 1: When $\lambda_{n,0}$ is fixed, θ_n increases with an increase in Γ_n^f, and $f_{4,n}\left(p_n^r, p_n^{BS}, \lambda_{n,0}, \theta_n\right)$ decreases with an increase in Γ_n^f.

Following Lemma 1, one property of the optimal solution to the problem P1 is further presented in what follows by Theorem 1, proven in Appendix B.

Theorem 1: If the problem P1 is feasible, the optimal solution to the problem P1 satisfies the constraint (14b) with equality.

According to Theorem 1, the variable p_n^{BS} in the problem P1 can be replaced with a function of p_n^r, given by

$$\begin{aligned} p_n^{BS} &= a_n p_n^r + b_n, \\ a_n &= \frac{\left(e^{C_n}-1\right)\left(h_n^{rtu}+h_n^{rcu}+h_n^{ru}\right)}{h_n^{bu}}, \\ b_n &= \frac{\left(e^{C_n}-1\right)\delta_n{}^2}{h_n^{bu}}. \end{aligned} \tag{16}$$

Equation (16) is derived from the constraint (14b) satisfied with equality. The maximum value of p_n^r is constrained with

$$p_n^r = \frac{p_n^{BS}-b_n}{a_n} \le \frac{p_{n,\max}^{BS}-b_n}{a_n}. \tag{17}$$

Based on Lemma 1 and Theorem 1, the monotonicity of $f_{4,n}\left(p_n^r, p_n^{BS}, \lambda_{n,0}, \theta_n\right)$ is provided in the following lemma, proven in Appendix C.

Lemma 2: When $\lambda_{n,0}$ is fixed, $f_{4,n}\left(p_n^r, p_n^{BS}, \lambda_{n,0}, \theta_n\right)$ decreases with an increase in p_n^r. When p_n^r is fixed, $f_{4,n}\left(p_n^r, p_n^{BS}, \lambda_{n,0}, \theta_n\right)$ increases with an increase in $\lambda_{n,0}$.

From the proof for Lemma 2, it is known that for a given transmit power p_n^r during one block, there exists a maximum EC during the block, denoted by $\lambda_{n,0}^{\max}$, that satisfies (14d) and (14e) with equality. $\lambda_{n,0}^{\max}$ can be obtained as follows. Considering that constraint (14e) is satisfied with equality, θ_n can be expressed in terms of $\lambda_{n,0}^{\max}$

$$\begin{aligned} \theta_n &= -\frac{1}{\lambda_{n,0}^{\max} d_{\max}} \ln\left\{\frac{p_0}{\lambda_{n,0}^{\max}} E\left\{B\ln\left(1+\Gamma_n^f\right)\right\}\right\} \\ &= -\frac{1}{\lambda_{n,0}^{\max} d_{\max}} \ln\left\{\frac{p_0 B}{\lambda_{n,0}^{\max}} E\left\{\ln\left(1+Z\right)\right\}\right\}, \end{aligned} \tag{18}$$

where

$$\begin{aligned} Z &= \frac{aX_1+bX_2+cX_3}{dX_4+kX_5+mX_6+1}, \\ a &= \frac{p_n^r \gamma_n^{rf}}{\delta_n{}^2}, \quad b = \frac{p_n^r \gamma_n^{rtf}}{\delta_n{}^2}, \\ c &= \frac{p_n^r \gamma_n^{rcf}}{\delta_n{}^2}, \quad d = \frac{p_n^{BS} \gamma_n^{btf}}{\delta_n{}^2}, \\ k &= \frac{p_n^{BS} \gamma_n^{bcf}}{\delta_n{}^2}, \quad m = \frac{p_n^{BS} \gamma_n^{bf}}{\delta_n{}^2}, \\ X_1 &= \alpha_n^{rf}, \quad X_2 = \alpha_n^{rtf}, \; X_3 = \alpha_n^{rcf}, \\ X_4 &= \alpha_n^{btf}, \quad X_5 = \alpha_n^{bcf}, \; X_6 = \alpha_n^{bf}. \end{aligned} \tag{19}$$

$E\left\{\ln\left(1+Z\right)\right\}$ is the ergodic capacity of the nth subcarrier, which can be obtained from Appendix D. Besides, $f_{3,n}\left(p_n^r, p_n^{BS}, \theta_n\right)$ can be expressed as

$$\begin{aligned} & f_{3,n}\left(p_n^r, p_n^{BS}, \theta_n\right) \\ &= -\frac{1}{\theta_n T} \ln E\left\{e^{-\theta_n TB \ln\left(1+\Gamma_n^f\left(p_n^r, p_n^{BS}\right)\right)}\right\} \\ &= -\frac{1}{\theta_n T} \ln E\left\{\left(1+Z\right)^{-\theta_n TB}\right\} \\ &= -\frac{1}{\theta_n T} \ln\left[\int_0^\infty \left(1+Z\right)^{-\theta_n TB} f_z\left(z\right) dz\right] \\ &= -\frac{1}{\theta_n T} \ln\left[\theta_n TB \int_0^\infty \frac{F_Z\left(Z\right)}{\left(1+Z\right)^{\theta_n TB+1}} dz\right], \end{aligned} \tag{20}$$

where $F_Z\left(Z\right)$ can be obtained from (61) in Appendix D. Moreover, the upper and lower bounds of $\lambda_{n,0}^{\max}$ can be obtained. As $\theta_n > 0$, according to (18), it follows that

$$\lambda_{n,0}^{\max} > p_0 BE\left\{\ln\left(1+Z\right)\right\}. \tag{21}$$

When $\theta_n = 0$, which means that the delay threshold is infinite, the EC is the same as the ergodic capacity [33], given by $BE\left\{\ln\left(1+Z\right)\right\}$. Considering that the EC is a monotonically decreasing function of θ_n [33], the range of EC can be given by

$$p_0 BE\left\{\ln\left(1+Z\right)\right\} < \lambda_{n,0}^{\max} < BE\left\{\ln\left(1+Z\right)\right\}. \tag{22}$$

Although there is no closed-form expression of the $f_{3,n}\left(p_n^r, p_n^{BS}, \theta_n\right)$, for a given p_n^r, when combining (18) and (20), and considering the constraint (14d), i.e., $f_{3,n}\left(p_n^r, p_n^{BS}, \theta_n\right) = \lambda_{n,0}^{\max}$, the bisection search algorithm over the interval in (22) can be applied to obtain $\lambda_{n,0}^{\max}$. Similarly, from Lemma 2, it can be obtained that when $\lambda_{n,0}$ is given, there exists a minimum value of p_n^r, denoted by $p_{n,\min}^r$, that satisfies constraints (14d) and (14e) with equality. The calculation of $p_{n,\min}^r$ is similar to that of $\lambda_{n,0}^{\max}$. In this paper, $p_{n,\min}^r$ is denoted as $p_{n,\min}^r = f_{5,n}\left(\lambda_{n,0}\right)$. Similarly, $\lambda_{n,0}^{\max}$ can be written as $\lambda_{n,0}^{\max} = f_{6,n}\left(p_n^r\right)$. Besides, $f_{6,n}\left(p_n^r\right)$ increases with p_n^r, which is proven in Appendix E.

Following from this observation, one property of the optimal solution to the problem P1 is presented in what follows by Theorem 2, proven in Appendix F.

Theorem 2: If the problem P1 is feasible, the constraints (14d), (14e), and (14f) can be replaced by

$$\sum_{n=0}^{N-1} f_{6,n}\left(p_n^r\right) \ge \lambda_0. \tag{23}$$

According to (16), p_n^{BS} is determined by p_n^r, thus, $f_{2,n}\left(p_n^r, p_n^{BS}\right)$ can be rewritten as $f_{2,n}\left(p_n^r\right)$. The problem P1 can be equivalently simplified to

$$(\boldsymbol{P2}): \min_{p_n^r} \sum_{n=0}^{N-1} p_n^r \tag{24a}$$

$$\sum_{n=0}^{N-1} f_{2,n}\left(p_n^r\right) \ge \phi_{MI} \tag{24b}$$

$$\sum_{n=0}^{N-1} f_{6,n}\left(p_n^r\right) \ge \lambda_0 \tag{24c}$$

$$0 \le p_n^r \le p_{n,\max}^{r'}, \tag{24d}$$

where $p_{n,\max}^{r'} = \min\left\{p_{n,\max}^r, \frac{p_{n,\max}^{BS}-b_n}{a_n}\right\}$, which is obtained by (14g) and (17). Besides, (14h) is guaranteed by (24d) when considering the relationship between p_n^{BS} and p_n^r in (16).

The increasing nature of the conditional MI with respect to p_n^r, and the decreasing nature of the second derivative of the conditional MI with respect to p_n^r are proven in Appendix G. Thus, the conditional MI, i.e., $f_{2,n}\left(p_n^r\right)$, is increasing and concave with respect to p_n^r. The maximum EC, i.e., $f_{6,n}\left(p_n^r\right)$, increases with p_n^r, as proven in Appendix E. However, the concavity of $f_{6,n}\left(p_n^r\right)$ is difficult to derive. According to [27], problem P2 is a monotonic minimization problem and can be easily transformed to a monotonic maximization problem P3 as follows:

$$(\boldsymbol{P3}): \max_{p_n^r} \sum_{n=0}^{N-1}\left(p_n^r - p_{n,\max}^{r'}\right) \tag{25a}$$

$$\phi_{MI} - \sum_{n=0}^{N-1} f_{2,n}\left(p_{n,\max}^{r'} - p_n^r\right) \le 0 \tag{25b}$$

$$\lambda_0 - \sum_{n=0}^{N-1} f_{6,n}\left(p_{n,\max}^{r'} - p_n^r\right) \le 0 \tag{25c}$$

$$0 \le p_n^r \le p_{n,\max}^{r'}, \tag{25d}$$

If problem P3 is feasible, the optimal result, given by p_n^{r*}, can be obtained through the polyblock outer approximation algorithm in [27]. By exploiting the special structure of the monotonic optimization problems, the computational complexity of the polyblock outer approximation algorithm involved in solving the problems is much more manageable than generic algorithms. However, the complexity is still high and can not be guaranteed within polynomial time [27]. Moreover, the optimal result can be classified as three cases.

Case 1: $\sum_{n=0}^{N-1} f_{6,n}\left(p_n^r\right) = \lambda_0$, and $\sum_{n=0}^{N-1} f_{2,n}\left(p_n^{r*}\right) = \phi_{MI}$.

Case 2: $\sum_{n=0}^{N-1} f_{6,n}\left(p_n^r\right) = \lambda_0$, and $\sum_{n=0}^{N-1} f_{2,n}\left(p_n^{r*}\right) > \phi_{MI}$.

Case 3: $\sum_{n=0}^{N-1} f_{6,n}\left(p_n^r\right) > \lambda_0$, and $\sum_{n=0}^{N-1} f_{2,n}\left(p_n^{r*}\right) = \phi_{MI}$.

Considering that $f_{2,n}\left(p_n^r\right)$ and $f_{6,n}\left(p_n^r\right)$ are monotonically increasing functions of p_n^r, the result that EC and MI are both over guaranteed does not exist. In Case 1, both the EC and MI are guaranteed with equality. In Case 2, MI is over guaranteed. In Case 3, EC is over guaranteed. From the above analysis, it is known that the communication performance for the fusion center and the detection performance are either or both guaranteed with minimum requirements.

Next, a special situation is considered, and a heuristic algorithm with low complexity is proposed to obtain the suboptimal result based on the special situation. Assuming that the EC on each subcarrier, i.e., $\lambda_{n,0}$, is given, the minimum power needed to satisfy $\lambda_{n,0}$ is $p_{n,\min}^r = f_{5,n}\left(\lambda_{n,0}\right)$. It follows that

$$\sum_{n=0}^{N-1} f_{6,n}\left(p_{n,\min}^r\right) = \lambda_0. \tag{26}$$

Considering that $f_{6,n}\left(p_n^r\right)$ is a monotonically increasing function of p_n^r, as proven in Appendix E, the problem P2 can be equivalently simplified to

$$(\boldsymbol{P4}): \min_{p_n^r} \sum_{n=0}^{N-1} p_n^r \tag{27a}$$

$$\sum_{n=0}^{N-1} f_{2,n}\left(p_n^r\right) \ge \phi_{MI} \tag{27b}$$

$$\boldsymbol{p}_{\min}^r \le \boldsymbol{p}^r \le \boldsymbol{p}_{\max}^{r'}, \tag{27c}$$

where $\boldsymbol{p}_{\min}^r$ and $\boldsymbol{p}_{\max}^{r'}$ are the sets of $p_{n,\min}^r$ and $p_{n,\max}^{r'}$, respectively. The objective function is affine, the MI constraint (27b) is concave, and the power constraint (27c) is convex. Therefore, the optimization problem P4 is convex and it is solvable under Karush-Kuhn-Tucker (KKT) conditions [23]. The method of Lagrange Multipliers is used to solve the problem P4, which is given by

$$L\left(p_n^r, \mu, \boldsymbol{\eta}, \boldsymbol{\varepsilon}\right) = \sum_{n=0}^{N-1} p_n^r + \mu\left(\phi_{MI} - \sum_{n=0}^{N-1} f_{2,n}\left(p_n^r\right)\right) + \boldsymbol{\eta}\left(\boldsymbol{p}_{\min}^r - \boldsymbol{p}^r\right) + \boldsymbol{\varepsilon}\left(\boldsymbol{p}^r - \boldsymbol{p}_{\max}^{r'}\right), \tag{28}$$

where $\mu \ge 0$, $\boldsymbol{\eta} \ge \boldsymbol{0}$, and $\boldsymbol{\varepsilon} \ge \boldsymbol{0}$ are the Lagrange multipliers for different constraints. The KKT conditions are given by

$$\frac{\partial L\left(p_n^r, \mu, \boldsymbol{\eta}, \boldsymbol{\varepsilon}\right)}{\partial p_n^r} = 1 - \mu^* f_{2,n}'\left(p_n^{r*}\right) - \eta_n^* + \varepsilon_n^* = 0 \tag{29a}$$

$$\boldsymbol{\eta}^*\left(\boldsymbol{p}_{\min}^r - \boldsymbol{p}^{r*}\right) = 0 \tag{29b}$$

$$\boldsymbol{\varepsilon}^*\left(\boldsymbol{p}^r - \boldsymbol{p}_{\max}^{r'}\right) = 0 \tag{29c}$$

$$\mu^*\left(\phi_{MI} - \sum_{n=0}^{N-1} f_{2,n}\left(p_n^{r*}\right)\right) = 0 \tag{29d}$$

$$p_{n,\min}^r \le p_n^r \le p_{n,\max}^{r'} \tag{29e}$$

$$\mu^* \ge 0, \quad \boldsymbol{\eta}^* \ge \boldsymbol{0}, \ \boldsymbol{\varepsilon}^* \ge \boldsymbol{0}. \tag{29f}$$

It is apparent from (29a), (29b), and (29c) that the optimal result can be separately investigated for three possibilities regarding the optimal allocated power on each subcarrier, i.e., $p_{n,\min}^r < p_n^r < p_{n,\max}^{r'}$, $p_n^r = p_{n,\min}^r$, and $p_n^r = p_{n,\max}^{r'}$.

If $p_{n,\min}^r < p_n^r < p_{n,\max}^{r'}$, then $\eta_n^* = 0, \varepsilon_n^* = 0$, and it follows that

$$f_{2,n}'\left(p_n^{r*}\right) = \frac{1}{\mu^*},$$
$$\frac{1}{f_{2,n}'\left(p_{n,\min}^r\right)} < \mu^* < \frac{1}{f_{2,n}'\left(p_{n,max}^r\right)}. \tag{30}$$

If $p_n^r = p_{n,\min}^r$, then $\eta_n^* > 0, \varepsilon_n^* = 0$, and it can be derived that

$$\mu^* \le \frac{1}{f_{2,n}'\left(p_{n,\min}^r\right)}. \tag{31}$$

If $p_n^r = p_{n,\max}^{r'}$, then $\eta_n^* = 0, \varepsilon_n^* > 0$, and it can be obtained that

$$\mu^* \ge \frac{1}{f_{2,n}'\left(p_{n,\max}^r\right)}. \tag{32}$$

Then, the optimal solution can be given by

$$p_n^{r*} = \begin{cases} p_{n,\min}^r, \mu^* \le \dfrac{1}{f_{2,n}'\left(p_{n,\min}^r\right)} \\ p_n^r\left(\dfrac{1}{\mu^*}\right), \dfrac{1}{f_{2,n}'\left(p_{n,\min}^r\right)} < \mu^* < \dfrac{1}{f_{2,n}'\left(p_{n,\max}^r\right)} \\ p_{n,\max}^{r'}, \mu^* \ge \dfrac{1}{f_{2,n}'\left(p_{n,\max}^r\right)}. \end{cases} \tag{33}$$

where $p_n^r\left(\frac{1}{\mu^*}\right)$ can be obtained by (71) in Appendix G. Besides, μ^* should satisfy

$$\sum_{n=0}^{N-1} f_{2,n}\left(p_n^{r*}\right) \ge \phi_{MI}. \tag{34}$$

The positive μ^* can be achieved by a simple bisection search over the interval $0 < \mu^* \le \min_n \frac{1}{f_{2,n}'(p_{n,\max}^r)}$. In the bisection search, (34) is used to verify whether μ^* is suitable for the solution. By now, the problem P4 has been solved with optimal result p_n^{r*}.

From the analysis above, it is shown that when the EC on each subcarrier is given, the optimal solution of problem P4 can be obtained. Thus, a heuristic algorithm is proposed to find out a suitable distribution of EC on each subcarrier. The pseudo code of the Heuristic Algorithm is presented in Algorithm 1. In the algorithm, parameter ρ is introduced to indicate the effect of conditional MI on the schedule result. If $\rho = 0$, it indicates that the EC distributed to the nth subcarrier is in proportion to the maximum EC of the nth subcarrier, i.e., $f_{6,n}\left(p_{n,\max}^r\right)$.

As the bisection search obtains $p_{n,\min}^r$, $\lambda_{n,0}^{\max}$, and solves problem P4 with complexity $O(\log(1/\varepsilon_0))$, the overall complexity of the heuristic algorithm is $O(200N\log(1/\varepsilon_0))$, where ε_0 is the error tolerance of the bisection search, which is set as $\varepsilon_0 = 10^{-6}$ in the simulations.

B. POWER ALLOCATION ALGORITHM WITH CHANNEL ESTIMATION ERROR

In Section III-A, the precise information of the slowly varying components of the channels is needed for the power allocation. However, the perfect knowledge of the channels is usually unavailable. The channel estimation error can be modeled as an additive white complex Gaussian random variable with a variance σ_e^2 with the conventional channel estimation methods, such as MMSE. However, the EC is difficult to derive when considering this model. Fortunately, the estimated channel power gain can also be assumed to lie between upper and lower bounds, which can be obtained through propagation modeling [2], [37], [38]. Note that a larger difference between the upper and lower bounds indicates greater uncertainty [37]. As an example, the upper and lower bounds of the channel power gain of the radar-target-radar channel are expressed as $\overline{h_n^{rtr}}$ and $\underline{h_n^{rtr}}$, respectively. The lower bound of the SINR of the radar signal in equation (3)

Algorithm 1 Heuristic Algorithm

Initialization:

Obtain the channel power gain, $\boldsymbol{p}_{\max}^{r'}, f_{6,n}\left(p_{n,\max}^{r'}\right)$, and ϕ_{MI}^0;

Set $\rho = 0$;

Iteration:

1: **while** $(0 \le \rho \le 1)$ **do**
2: Set $\boldsymbol{p}_{\min}^r = \mathbf{0}$ and $\phi_{MI} = 2\rho\phi_{MI}^0/B$.
3: Obtain the optimal result of problem P4 with parameters $\boldsymbol{p}_{\min}^r$, ϕ_{MI} and $\boldsymbol{p}_{\max}^{r'}$, given as p_n^r;
4: Obtain the available EC, i.e., $f_{6,n}\left(p_n^r\right)$, with $p_n^r > 0, n \in N'$;
5: Allocate the residual EC to the subcarrier with $p_n^r = 0$ according to $f_{6,n}\left(p_{n,\max}^{r'}\right)$,
$\lambda_{n,0} = \frac{f_{6,n}\left(p_{n,\max}^{r'}\right)}{\sum_{n\in N/N'} f_{6,n}\left(p_{n,\max}^{r'}\right)}\left(\lambda_0 - \sum_{n\in N'} f_{6,n}\left(p_n^r\right)\right)$,
$n \in N/N'$;
6: Obtain the minimum power needed for the EC on subcarrier n, $n \in N/N'$,
$p_{n,\min}^r = f_{5,n}\left(\lambda_{n,0}\right), n \in N/N'$;
7: Update the power on each subcarrier,
$p_{n,\min}^r = p_{n,\min}^r + p_n^r$;
8: Set $\phi_{MI} = 2\phi_{MI}^0/B$ and obtain the optimal result of problem P4 with parameters $p_{n,\min}^r$, ϕ_{MI} and $\boldsymbol{p}_{\max}^{r'}$;
9: $\rho = \rho + 0.01$;
10: **end while**
11: Obtain the minimum $\sum_{n=0}^{N-1} p_n^r$.

can be obtained

$$\underline{\Gamma_n^r} = \frac{p_n^r \underline{h_n^{rtr}}}{p_n^r \overline{h_n^{rcr}} + p_n^{BS}\left(\overline{h_n^{btr}} + \overline{h_n^{bcr}} + \overline{g_n^{br}}\right) + \delta_n^2}. \tag{35}$$

The lower bound of the SINR of the fusion center and BS user can be derived in the same way, which are denoted as $\underline{\Gamma_n^f}$ and $\underline{\Gamma_n^{BS}}$, respectively.

$$\underline{\Gamma_n^f} = \frac{p_n^r\left(\underline{\gamma_n^{rf}}\alpha_n^{rf} + \underline{\gamma_n^{rtf}}\alpha_n^{rtf} + \underline{\gamma_n^{rcf}}\alpha_n^{rcf}\right)}{p_n^{BS}\left(\overline{\gamma_n^{btf}}\alpha_n^{btf} + \overline{\gamma_n^{bcf}}\alpha_n^{bcf} + \overline{\gamma_n^{bf}}\alpha_n^{bf}\right) + \delta_n^2}, \tag{36}$$

$$\underline{\Gamma_n^{BS}} = \frac{p_n^{BS}\underline{h_n^{bu}}}{p_n^r\left(\overline{h_n^{rtu}} + \overline{h_n^{rcu}} + \overline{h_n^{ru}}\right) + \delta_n^2}. \tag{37}$$

As described in [37], the robust power allocation is the optimal power allocation for the worst-case channel power gain. Substituting $\underline{\Gamma_n^r}$, $\underline{\Gamma_n^f}$, and $\underline{\Gamma_n^{BS}}$ into the constraints in problem P1, a robust power allocation can be obtained with the method in Section III-A. For simplicity, a ratio δ is defined, and the upper and lower bounds in equations (35)-(37) are related

TABLE 1. Simulation parameters.

Symbol	Value	Symbol	Value	Symbol	Value
G_t	40dB	d_{bt}	50km	T	1ms
G_r	40dB	d_{bf}	10.051km	$d_{\max}$	1ms
G_s	0dB	d_{bu}	200m	p_0	0.001
d_{rt}	50km	d_{ft}	50km	N	128
d_{rf}	10.051km	$p^r_{n,\max}$	300W	${\delta_n}^2$	-114dBm
d_{br}	20km	p^{BS}_{total}	20W	ξ	4dBm

with δ, which are given by

$$\begin{aligned}
\underline{h_n^{rtr}} &= (1-0.5\delta)h_n^{rtr},\\
\overline{h_n^{rcr}} &= (1+0.5\delta)h_n^{rcr},\\
\overline{h_n^{btr}} &= (1+0.5\delta)h_n^{btr},\\
\overline{h_n^{bcr}} &= (1+0.5\delta)h_n^{bcr},\\
\overline{g_n^{br}} &= (1+0.5\delta)g_n^{br}. \qquad (38)\\
\underline{\gamma_n^{rf}} &= (1-0.5\delta)\gamma_n^{rf},\\
\underline{\gamma_n^{rtf}} &= (1-0.5\delta)\gamma_n^{rtf},\\
\underline{\gamma_n^{rcf}} &= (1-0.5\delta)\gamma_n^{rcf},\\
\overline{\gamma_n^{btf}} &= (1+0.5\delta)\gamma_n^{btf},\\
\overline{\gamma_n^{bcf}} &= (1+0.5\delta)\gamma_n^{bcf},\\
\overline{\gamma_n^{bf}} &= (1+0.5\delta)\gamma_n^{bf}. \qquad (39)\\
\underline{h_n^{bu}} &= (1-0.5\delta)h_n^{bu},\\
\overline{h_n^{rtu}} &= (1+0.5\delta)h_n^{rtu},\\
\overline{h_n^{rcu}} &= (1+0.5\delta)h_n^{rcu},\\
\overline{h_n^{ru}} &= (1+0.5\delta)h_n^{ru}. \qquad (40)
\end{aligned}$$

When $\delta = 0$, it means that the precise channel information is available. Besides, a larger δ indicates a greater gap between the upper and lower bounds.

IV. SIMULATION

This section first provides numerical results to show the upper and lower bounds of the EC. Then, the power allocation results and the power-saving performance of the proposed heuristic algorithm are demonstrated, and compared with the theoretical result. In all the simulations, the extended target is considered, the carrier frequency of the IRCS is 3 GHz, and the bandwidth of each subcarrier is 4 MHz, i.e., $B = 4$ MHz. Other simulation parameters are shown in Table 1. As previously mentioned, to solve the resulting optimization problem (P1), it is assumed that the fusion center knows the slowly varying components of the channels by sensing and feedback [2], [3], [8], [29], [30]. Thus, the slowly varying components of the target channels, clutters channels and direct paths are illustrated in Fig. 2, Fig. 3, and Fig. 4. When the transmit power is determined, the SINRs of the radar signal in (3) and BS user in (13) can be obtained. For comparison, one benchmark is applied. In this method, the total EC is equally allocated to different subcarriers, i.e., $\lambda_{n,0} = \lambda_0/N$, which is named as EQ. With the given

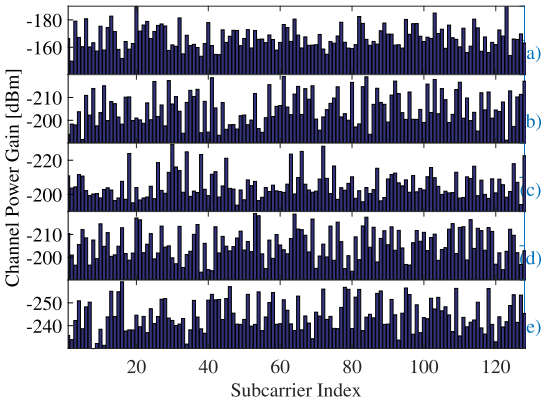

FIGURE 2. The slowly varying components of the target channels: a) h_n^{rtr}; b)h_n^{btr}; c)h_n^{rtu}; d)γ_n^{rtf}; e)γ_n^{btf}.

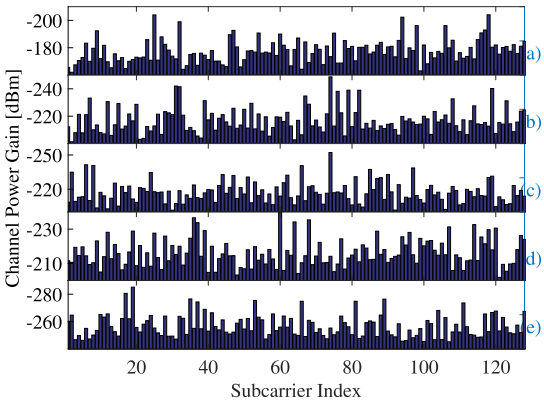

FIGURE 3. The slowly varying components of the clutter channels: a) h_n^{rcr}; b)h_n^{bcr}; c)h_n^{rcu}; d)γ_n^{rcf}; e)γ_n^{bcf}.

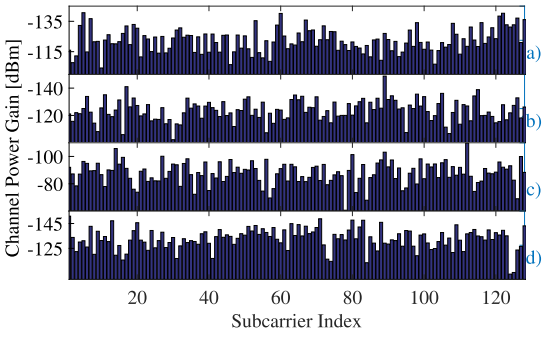

FIGURE 4. The slowly varying components of the direct paths: a) γ_n^{rf}; b)γ_n^{bf}; c)h_n^{bu}; d)h_n^{ru}.

$\lambda_{n,0}$, the optimal result of problem P4 stands for the power allocation scheme of the benchmark. The complexity of the benchmark is $O\left(N \log\left(1/\varepsilon_0\right)\right)$, where ε_0 is the error tolerance of the bisection search in problem P4.

A. THE UPPER AND LOWER BOUNDS OF THE EC

The effects of LVP and transmit power to the maximum EC are illustrated in Fig. 5. It is shown that the maximum EC monofonically increases with an increase in transmitted

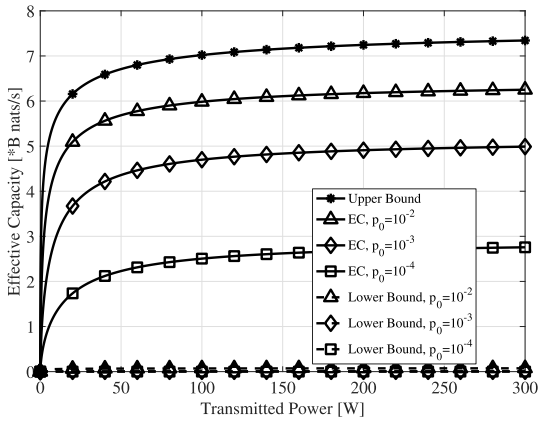

FIGURE 5. The maximum EC with varying transmit power.

power, which is proven in Appendix E, and the tendency is similar to the upper bound, i.e., ergodic capacity. With a smaller LVP, the requirement on the EC is more stringent, which results in a smaller maximum EC, as demonstrated in the simulation. Moreover, the maximum EC is always between the upper bound and lower bound, which is consistent with our analysis.

B. PERFORMANCE OF POWER ALLOCATION

Fig. 6 compares the power allocation results of the theoretical solution, heuristic algorithm, and EQ. The rate requirement of the BS user is $C_n^0 = B$ nats/s, the minimum MI required is $\phi_{MI}^0 = 7.5B$ nats/s, and the minimum EC required is $\lambda_0 = 2NB$ nats/s. Besides, the LVP should be no more than $p_0 = 10^{-3}$ with the latency bounded by $d_{\max} = 1$ ms. The theoretical solution, heuristic algorithm, and EQ only concentrate the transmit power on a small fraction of the channels. Moreover, the LVPs of the theoretical solution and heuristic algorithm are very close to $p_0 = 10^{-3}$, which indicates that the maximum EC of the two methods are close to the requirement. On the contrary, the LVP of the EQ is over guaranteed for some subcarriers, resulting in a waste of power. When compared with the theoretical solution, the total power of heuristic algorithm and EQ increase by about 2.48% and 10.81%, respectively.

Fig. 7 shows the total transmit power versus the EC under different MI requirements. Considering the optimal solution when $\phi_{MI}^0 = 5B$ nats/s, the EC and conditional MI are satisfied with equality when $0.3NB \le \lambda_0 \le 2.3NB$ nats/s, MI is over guaranteed with $\lambda_0 > 2.3NB$ nats/s, and EC is over satisfied when $\lambda_0 \le 0.2NB$ nats/s, corresponding to the Case 1, 2, and 3 of the optimal solution, respectively. The results of the heuristic algorithm and the optimal result are close when considering the total transmit power, maximum EC, and maximum MI. However, the EC of the EQ algorithm is always over guaranteed, which results in the degradation of performance. When $\phi_{MI}^0 = 5B$ nats/s, with the EC from $0.4NB$ to $1.6NB$ nats/s, the total transmit power of the heuristic algorithm and EQ increase by about 2.42% and

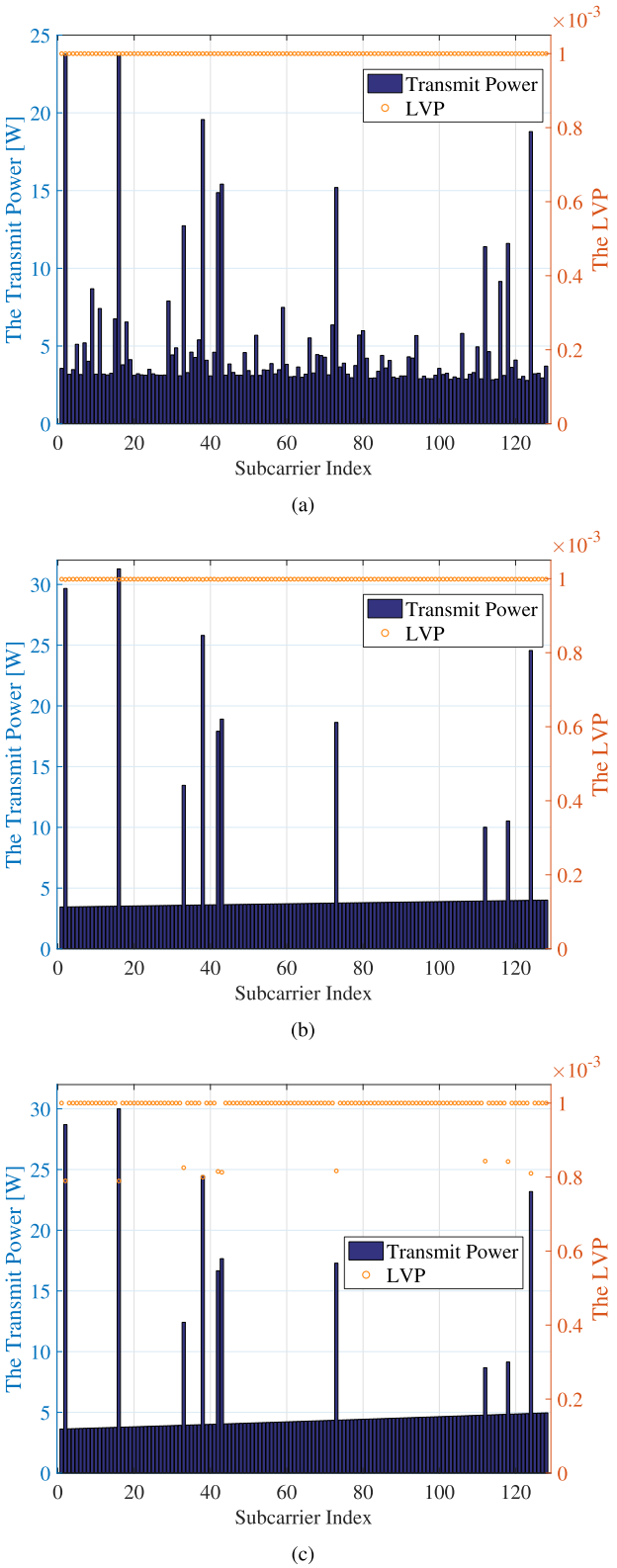

FIGURE 6. The power allocation result. (a) The theoretical solution. (b) The proposed algorithm. (c) The EQ algorithm.

14.03% when compared with the optimal solution. Similarly, the gaps are about 2.19% and 12.53% when $\phi_{MI}^0 = 9B$ nats/s. Fig. 8 demonstrates the similar results. From these

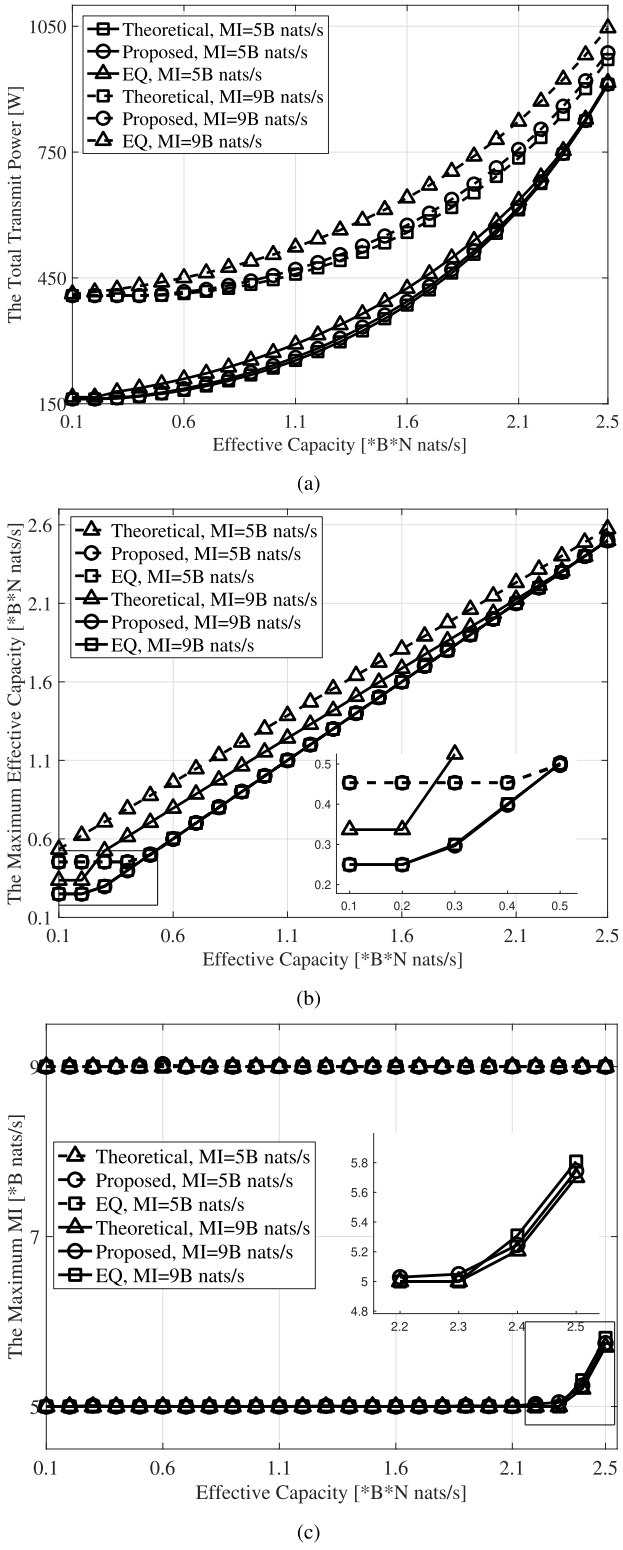

FIGURE 7. The power allocation result with varying total EC. (a) Total transmit power. (b) Maximum EC. (c) Maximum MI.

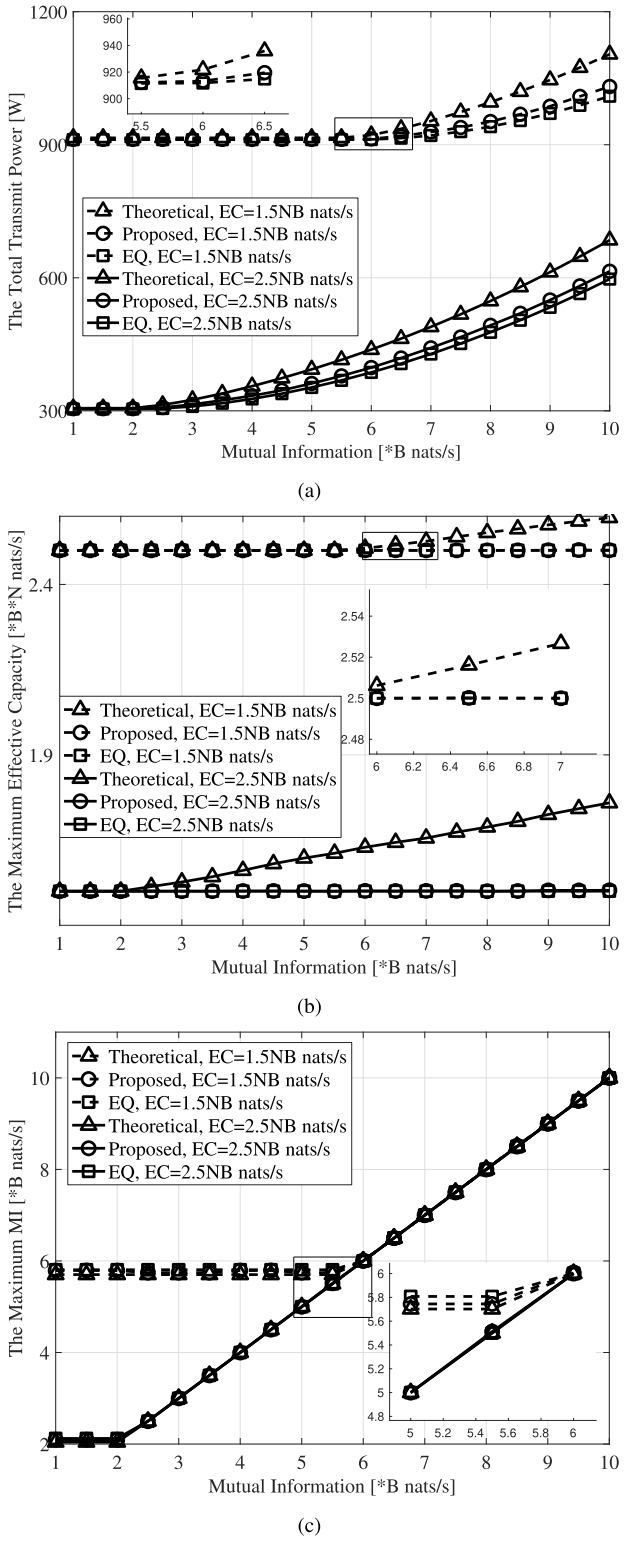

FIGURE 8. The power allocation result with varying conditional MI. (a) Total transmit power. (b) Maximum EC. (c) Maximum MI.

simulations, the proper requirements of EC and MI can be obtained to satisfy constraints (24b) and (24c) with equality, which can maximize the efficiency of the transmit power.

By varying the latency bound $d_{\max}$ of the A2G communication, Fig. 9 demonstrates the total transmit power for different LVP requirements. The MI and EC requirements are

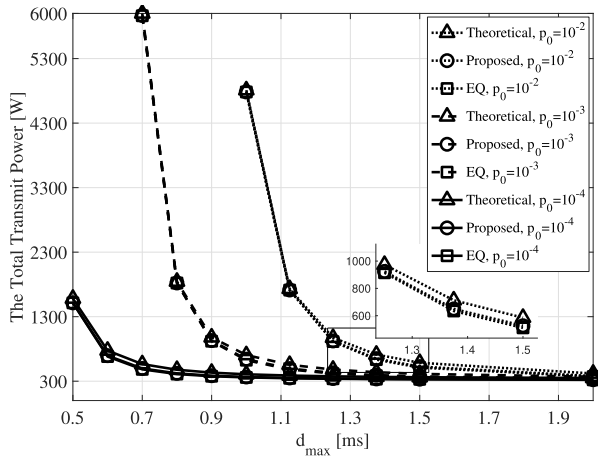

(a)

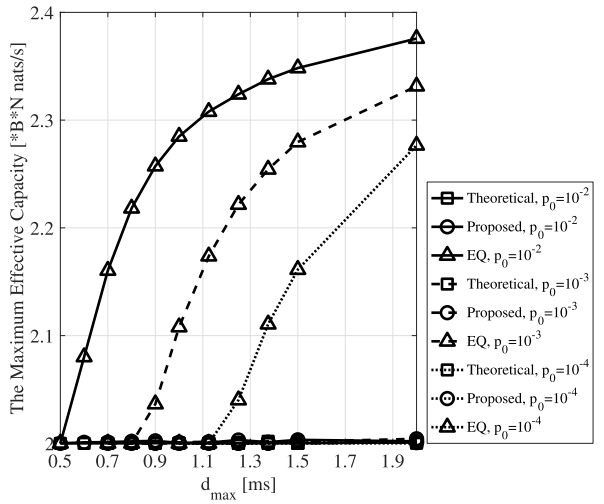

(b)

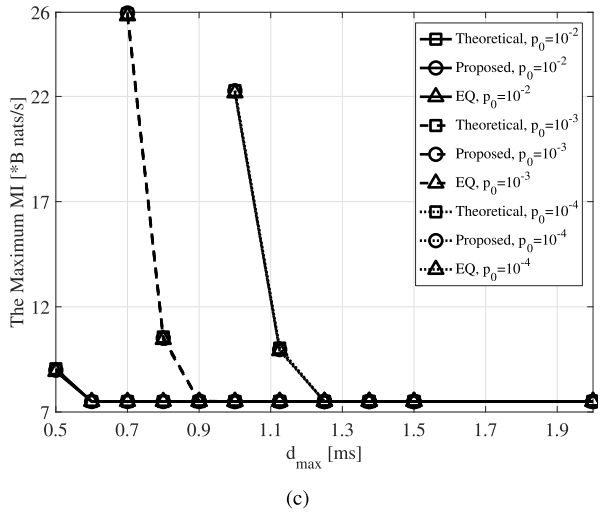

(c)

FIGURE 9. The power allocation result with varying latency bounds. (a) Total transmit power. (b) Maximum EC. (c) Maximum MI.

the same as the ones in Fig. 6. With increased $d_{\max}$ or p_0, the same EC can be achieved with smaller p_n^r, thus, the total transmit power decreases with an increase in $d_{\max}$ and p_0.

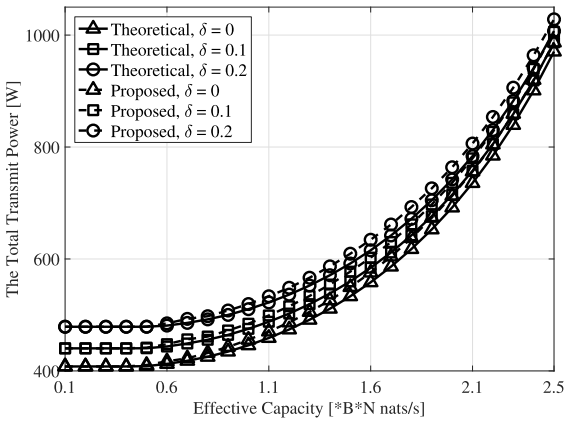

FIGURE 10. The power allocation result with channel estimation error.

When $d_{\max}$ or p_0 is small, the power needed to guarantee the LVP is quite large, and the MI requirement is over satisfied, which is the Case 2. The transmit power is determined by both the MI and EC requirements when $d_{\max}$ is large, which is the Case 1.

The effects of channel estimation error are illustrated in Fig. 10. The minimum required MI is $\phi_{MI}^0 = 9B$ nats/s, and the range of EC is $0.1NB \leq \lambda_0 \leq 2.5NB$ nats/s. Other parameters are the same as the ones in Fig. 6. The ratio δ in equations (38)-(40) is set as 0, 0.1, and 0.2 in the simulation. Compared with the situation that $\delta = 0$, the total transmit power of the theoretical solution increases by about 5.39% when $\delta = 0.1$ and about 11.85% when $\delta = 0.2$, respectively. The proposed algorithm has a similar tendency. Moreover, considering the theoretical solution with $\lambda_0 = 2.5NB$ nats/s, the total transmit power only increases by about 3.78% when $\delta = 0.1$ and about 5.94% when $\delta = 0.2$, respectively. This indicates that the system is less sensitive to the channel estimation error when the EC requirement is larger.

V. CONCLUSION

In this paper, the problem of power minimization based IRCS power allocation for spectrum sharing with the BS was studied. The detection performance for radar, the LVP for the A2G communication to the fusion center, and the rate requirement of BS user were considered, where the LVP was expressed by the EC theory. Firstly, the optimal power allocation scheme was designed for minimizing the consumed energy. Then, the problem was simplified to concise form, and a low-complexity heuristic algorithm was proposed to obtain the sub-optimal result. Besides, the effect of channel estimation error is considered in the robust power allocation algorithm. Finally, the effectiveness of the heuristic algorithm was demonstrated by the numerical results. In the future, a multiple-antenna system may be taken into consideration, and the transmit beamforming and power allocation be jointly optimized.

APPENDIX A
PROOF OF LEMMA 1

Assuming that $\Gamma_n^f\left(p_n^{r'}, p_n^{BS'}\right) > \Gamma_n^f\left(p_n^r, p_n^{BS}\right)$, it is not difficult to obtain

$$E\left\{\ln\left(1+\Gamma_n^f\left(p_n^{r'}, p_n^{BS'}\right)\right)\right\} > E\left\{\ln\left(1+\Gamma_n^f\left(p_n^r, p_n^{BS}\right)\right)\right\} \tag{41}$$

and

$$-\frac{1}{\theta_n T}\ln E\left\{e^{-\theta_n TB\ln\left(1+\Gamma_n^f\left(p_n^{r'}, p_n^{BS'}\right)\right)}\right\} > -\frac{1}{\theta_n T}\ln E\left\{e^{-\theta_n TB\ln\left(1+\Gamma_n^f\left(p_n^r, p_n^{BS}\right)\right)}\right\} = \lambda_{n,0}. \tag{42}$$

As the EC function $f_{3,n}\left(p_n^r, p_n^{BS}, \theta_n\right)$ is monotonically decreasing with θ_n [33], to guarantee

$$-\frac{1}{\theta_n' T}\ln E\left\{e^{-\theta_n' TB\ln\left(1+\Gamma_n^f\left(p_n^{r'}, p_n^{BS'}\right)\right)}\right\} = \lambda_{n,0}, \tag{43}$$

$\theta_n' > \theta_n$ must be satisfied. When jointly considering (41) and $\theta_n' > \theta_n$, it can be obtained that

$$\frac{\lambda_{n,0}}{E\left\{B\ln\left(1+\Gamma_n^f\left(p_n^{r'}, p_n^{BS'}\right)\right)\right\}} e^{-\theta_n'\lambda_{n,0}d_{\max}} < \frac{\lambda_{n,0}}{E\left\{B\ln\left(1+\Gamma_n^f\left(p_n^r, p_n^{BS}\right)\right)\right\}} e^{-\theta_n\lambda_{n,0}d_{\max}}. \tag{44}$$

APPENDIX B
PROOF OF THEOREM 1

Assuming that $\left(p_n^{r*}, p_n^{BS*}, \theta_n^*, \lambda_{n,0}^*\right)$ is the optimal solution, and $f_{1,n}\left(p_n^{r*}, p_n^{BS*}\right) > C_n$, $C_n = C_n^0/B$. When the optimal transmit power of the BS is slightly decreased to $p_n^{BS'} = \mu_1 p_n^{BS*}, 0 < \mu_1 < 1$, the μ_1 that satisfies $f_{1,n}\left(p_n^{r*}, p_n^{BS'}\right) = C_n$ can be obtained. It follows that

$$\begin{aligned}\Gamma_n^r\left(p_n^{r*}, p_n^{BS'}\right) &> \Gamma_n^r\left(p_n^{r*}, p_n^{BS*}\right),\\ \Gamma_n^f\left(p_n^{r*}, p_n^{BS'}\right) &> \Gamma_n^f\left(p_n^{r*}, p_n^{BS*}\right).\end{aligned} \tag{45}$$

Assuming that $p_n^{r'} = \mu_2 p_n^{r*}, 0 < \mu_2 < 1$, and $p_n^{r''} = \mu_3 p_n^{r*}, 0 < \mu_3 < 1$, there exist μ_2 and μ_3 that satisfy

$$\begin{aligned}\Gamma_n^r\left(p_n^{r'}, p_n^{BS'}\right) &= \Gamma_n^r\left(p_n^{r*}, p_n^{BS*}\right),\\ \Gamma_n^f\left(p_n^{r''}, p_n^{BS'}\right) &= \Gamma_n^f\left(p_n^{r*}, p_n^{BS*}\right).\end{aligned} \tag{46}$$

Set $p_n^{r'''} = \max\left\{p_n^{r'}, p_n^{r''}\right\}$, from Lemma 1, it can be obtained that

$$\begin{aligned}f_{1,n}\left(p_n^{r'''}, p_n^{BS'}\right) &\geq f_{1,n}\left(p_n^{r*}, p_n^{BS*}\right),\\ f_{3,n}\left(p_n^{r'''}, p_n^{BS'}, \theta_n'\right) &= f_{3,n}\left(p_n^{r*}, p_n^{BS*}, \theta_n^*\right) = \lambda_{n,0},\\ \theta_n' &\geq \theta_n^*,\\ f_{4,n}\left(p_n^{r'''}, p_n^{BS'}, \theta_n', \lambda_{n,0}^*\right) &\leq f_{4,n}\left(p_n^{r*}, p_n^{BS*}, \theta_n^*, \lambda_{n,0}^*\right).\end{aligned} \tag{47}$$

Then, $\left(p_n^{r'''}, p_n^{BS'}, \lambda_{n,0}^*, \theta_n'\right)$ is the feasible solution and has a smaller objective value than $\left(p_n^{r*}, p_n^{BS*}, \lambda_{n,0}^*, \theta_n^*\right)$. Thus, $\left(p_n^{r*}, p_n^{BS*}, \lambda_{n,0}^*, \theta_n^*\right)$ is not the optimal solution. This is a contradiction and the optimal solution must satisfy the constraint (14b) with equality.

APPENDIX C
PROOF OF LEMMA 2

Set $p_n^{r'} = \eta p_n^r$, $1 < \eta < \frac{p_{n,\max}^r}{p_n^r}$, combining (7) and (16), it can be derived that

$$\Gamma_n^f\left(p_n^{r'}, p_n^{BS'}\right) > \Gamma_n^f\left(p_n^r, p_n^{BS}\right). \tag{48}$$

From Lemma 1, it follows that

$$f_{4,n}\left(p_n^{r'}, p_n^{BS'}, \lambda_{n,0}, \theta_n'\right) < f_{4,n}\left(p_n^r, p_n^{BS}, \lambda_{n,0}, \theta_n\right). \tag{49}$$

Set

$$f_{3,n}\left(p_n^r, p_n^{BS}, \theta_n\right) = \lambda_{n,0} \tag{50a}$$

$$f_{3,n}\left(p_n^r, p_n^{BS}, \theta_n'\right) = \lambda_{n,0}' \tag{50b}$$

$$\lambda_{n,0}' = \mu\lambda_{n,0}, \quad 1 < \mu < \frac{\lambda_0}{\lambda_{n,0}}. \tag{50c}$$

As $f_{3,n}\left(p_n^r, p_n^{BS}, \theta_n\right)$ is a monotonically decreasing function of θ_n, it can be obtained that

$$\theta_n' < \theta_n \tag{51a}$$

$$\begin{aligned}\theta_n'\lambda_{n,0}' &= -\frac{1}{T}\ln E\left\{e^{-\theta_n' TB\ln\left(1+\Gamma_n^f\right)}\right\}\\ &< -\frac{1}{T}\ln E\left\{e^{-\theta_n TB\ln\left(1+\Gamma_n^f\right)}\right\} = \theta_n\lambda_{n,0}.\end{aligned} \tag{51b}$$

When combing (50c) and (51b), it follows that

$$\begin{aligned}f_{4,n}\left(p_n^r, p_n^{BS}, \theta_n', \lambda_{n,0}'\right) &= \frac{\lambda_{n,0}'}{E\left\{B\ln\left(1+\Gamma_n^f\right)\right\}} e^{-\theta_n'\lambda_{n,0}'d_{\max}}\\ &> \frac{\lambda_{n,0}}{E\left\{B\ln\left(1+\Gamma_n^f\right)\right\}} e^{-\theta_n\lambda_{n,0}d_{\max}}\\ &= f_{4,n}\left(p_n^r, p_n^{BS}, \theta_n, \lambda_{n,0}\right).\end{aligned} \tag{52}$$

From the analysis above, it is known that when p_n^r is given, there exists a maximum value of μ, denoted by $\mu_{\max}$, that satisfies constraint (14e) with equality. It indicates the maximum EC, denoted by $\lambda_{n,0}^{\max}$, can be achieved with p_n^r. Constraint (14d) is also guaranteed according to (50b).

APPENDIX D
ERGODIC CAPACITY OF THE IRCS ON THE *n*th SUBCARRIER

The ergodic capacity of the IRCS on the nth subcarrier, i.e., $E\{\ln(1+Z)\}$ can be written as

$$E\{\ln(1+Z)\} = E\left\{\ln\left(\frac{1+aX_1+bX_2+cX_3}{dX_4+kX_5+mX_6+1}\right)\right\}, \tag{53}$$

where

$$a = \frac{p_n^r \gamma_n^{rf}}{{\delta_n}^2}, \quad b = \frac{p_n^r \gamma_n^{rtf}}{{\delta_n}^2}, \; c = \frac{p_n^r \gamma_n^{rcf}}{{\delta_n}^2},$$
$$d = \frac{p_n^{BS} \gamma_n^{btf}}{{\delta_n}^2}, \quad k = \frac{p_n^{BS} \gamma_n^{bcf}}{{\delta_n}^2}, \; m = \frac{p_n^{BS} \gamma_n^{bf}}{{\delta_n}^2}. \quad (54)$$

$\alpha_n^{rf}, \alpha_n^{rtf}, \alpha_n^{rcf}, \alpha_n^{btf}, \alpha_n^{bcf}$, and α_n^{bf} are denoted as X_1, X_2, X_3, X_4, X_5 and X_6, respectively. Defining $Y_1 = aX_1, Y_2 = bX_2, Y_3 = cX_3, Y_4 = dX_4, Y_5 = kX_5, Y_6 = mX_6$, and considering that $\alpha_n^{rf}, \alpha_n^{rtf}, \alpha_n^{rcf}, \alpha_n^{btf}, \alpha_n^{bcf}$, and α_n^{bf} are i.i.d. exponential random variables with unit mean, their probability density functions (PDFs) are given by

$$f_{y_1}(y_1) = \frac{1}{a} e^{-\frac{y_1}{a}}, \quad f_{y_2}(y_2) = \frac{1}{b} e^{-\frac{y_2}{b}}, \; f_{y_3}(y_3) = \frac{1}{c} e^{-\frac{y_3}{c}},$$
$$f_{y_4}(y_4) = \frac{1}{d} e^{-\frac{y_4}{d}}, \quad f_{y_5}(y_5) = \frac{1}{k} e^{-\frac{y_5}{k}}, \; f_{y_6}(y_6) = \frac{1}{m} e^{-\frac{y_6}{m}}. \quad (55)$$

Defining $U = Y_1 + Y_2$, its cumulative distribution function (CDF) and PDF are

$$\begin{aligned} F_U(U) &= p(Y_1 + Y_2 \le u) \\ &= \int_0^u d_{y_1} \int_0^{u-y_1} \frac{1}{ab} e^{-\left(\frac{y_1}{a} + \frac{y_2}{b}\right)} d_{y_2} \\ &= 1 - \frac{a}{a-b} e^{-\frac{u}{a}} - \frac{b}{b-a} e^{-\frac{u}{b}}, \\ f_u(u) &= F_U'(U) = \frac{1}{a-b}\left(e^{-\frac{u}{a}} - e^{-\frac{u}{b}}\right). \end{aligned} \quad (56)$$

Defining $V = U + Y_3$, the CDF and PDF are given by

$$\begin{aligned} F_V(V) &= p(U + Y_3 \le v) \\ &= \int_0^v d_u \int_0^{v-u} \frac{1}{a-b}\left(e^{-\frac{u}{a}} - e^{-\frac{u}{b}}\right) \frac{1}{c} e^{-\frac{y_3}{c}} d_{y_3} \\ &= 1 - a_1 e^{-\frac{v}{a}} - b_1 e^{-\frac{v}{b}} - c_1 e^{-\frac{v}{c}}, \\ f_v(v) &= \frac{a_1}{a} e^{-\frac{v}{a}} + \frac{b_1}{b} e^{-\frac{v}{b}} + \frac{c_1}{c} e^{-\frac{v}{c}}, \end{aligned} \quad (57)$$

where

$$a_1 = \frac{a^2}{(a-b)(a-c)}, \quad b_1 = \frac{b^2}{(b-a)(b-c)},$$
$$c_1 = \frac{c^2}{(c-a)(c-b)}, \quad a_1 + b_1 + c_1 = 1. \quad (58)$$

Similarly, defining $W = Y_4 + Y_5 + Y_6$, the PDF of w is

$$f_w(w) = \frac{d_1}{d} e^{-\frac{w}{d}} + \frac{k_1}{k} e^{-\frac{w}{k}} + \frac{m_1}{m} e^{-\frac{w}{m}}, \quad (59)$$

where

$$d_1 = \frac{d^2}{(d-k)(d-m)}, \quad k_1 = \frac{k^2}{(k-d)(k-m)},$$
$$m_1 = \frac{m^2}{(m-d)(m-k)}, \quad d_1 + k_1 + m_1 = 1. \quad (60)$$

Defining $Z = \frac{V}{W+1}$, its CDF is given by

$$\begin{aligned} F_Z(Z) &= p\left(\frac{V}{W+1} \le z\right) \\ &= \int_0^\infty d_w \int_0^{z(w+1)} f_w(w) f_v(v) d_v \\ &= 1 - e^{-\frac{z}{a}}\left(\frac{aa_1d_1}{a+dz} + \frac{aa_1k_1}{a+kz} + \frac{aa_1m_1}{a+mz}\right) \\ &\quad - e^{-\frac{z}{b}}\left(\frac{bb_1d_1}{b+dz} + \frac{bb_1k_1}{b+kz} + \frac{bb_1m_1}{b+mz}\right) \\ &\quad - e^{-\frac{z}{c}}\left(\frac{cc_1d_1}{c+dz} + \frac{cc_1k_1}{c+kz} + \frac{cc_1m_1}{c+mz}\right) \end{aligned} \quad (61)$$

Then, the ergodic capacity of the IRCS for the nth subcarrier, i.e., $E\{\ln(1+Z)\}$, is derived

$$\begin{aligned} E\{\ln(1+Z)\} &= \int_0^\infty \ln(1+z) f_z(z) \, d_z \\ &= \int_0^\infty \ln(1+z) F_Z'(Z) \, d_z \\ &= \int_0^\infty \frac{1 - F_Z(Z)}{z+1} d_z \end{aligned} \quad (62)$$

A numerical result for $E\{\ln(1+Z)\}$ can be obtained when (61) and (62) are combined.

APPENDIX E
THE MONOTONICITY OF $f_{6,n}(p_n^r)$

Similar to the proof for Lemma 2, set $p_n^{r'} = \eta p_n^r$, $1 < \eta < \frac{p_{n,\max}^r}{p_n^r}$, it follows that

$$f_{3,n}\left(p_n^r, p_n^{BS}, \theta_n\right) = \lambda_{n,0}^{\max} \quad (63a)$$
$$f_{4,n}\left(p_n^r, p_n^{BS}, \theta_n, \lambda_{n,0}^{\max}\right) = p_0 \quad (63b)$$
$$f_{3,n}\left(p_n^{r'}, p_n^{BS'}, \theta_n'\right) = \lambda_{n,0}^{\max'} \quad (63c)$$
$$f_{4,n}\left(p_n^{r'}, p_n^{BS'}, \theta_n', \lambda_{n,0}^{\max'}\right) = p_0. \quad (63d)$$

Assuming that $\lambda_{n,0}^{\max'} \le \lambda_{n,0}^{\max}$, it can be derived that

$$\begin{aligned} \theta_n' &\ge \theta_n, \\ \theta_n' \lambda_{n,0}^{\max'} &= -\frac{1}{T} \ln E\left\{e^{-\theta_n' TB \ln\left(1+\Gamma_n^{f'}\right)}\right\} \\ &> \theta_n \lambda_{n,0}^{\max}. \end{aligned} \quad (64)$$

According to Lemma 2, it can be obtained that

$$\begin{aligned} f_{4,n}\left(p_n^{r'}, p_n^{BS'}, \theta_n', \lambda_{n,0}^{\max'}\right) &< f_{4,n}\left(p_n^r, p_n^{BS}, \theta_n', \lambda_{n,0}^{\max'}\right) \\ &< f_{4,n}\left(p_n^r, p_n^{BS}, \theta_n, \lambda_{n,0}^{\max}\right) \\ &= p_0. \end{aligned} \quad (65)$$

As a result, (63d) cannot be satisfied. Thus, $\lambda_{n,0}^{\max'} > \lambda_{n,0}^{\max}$ must hold.

APPENDIX F
PROOF OF THEOREM 2

Considering that $\sum_{n=0}^{N-1} f_{6,n}\left(p_n^{r*}\right) \geq \lambda_0$, one optimal EC on each subcarrier can be given by

$$\lambda_{n,0}^{*} = \lambda_0 \frac{f_{6,n}\left(p_n^{r*}\right)}{\sum_{n=0}^{N-1} f_{6,n}\left(p_n^{r*}\right)} \leq \lambda_{n,0}^{\max}. \tag{66}$$

From the process of proof for Lemma 2 in Appendix C, $\mu_{1,n} \leq \mu_{1,n}^{\max}$ is satisfied, which indicates that

$$\begin{aligned} f_{3,n}\left(p_n^{r*}, p_n^{BS*}, \theta_n^{*}\right) &= \lambda_{n,0}^{*}, \\ f_{4,n}\left(p_n^{r*}, p_n^{BS*}, \theta_n^{*}, \lambda_{n,0}^{*}\right) &\leq p_0. \end{aligned} \tag{67}$$

Thus, constraints (14d), (14e) and (14f) are all satisfied.

Considering that constraints (14d), (14e) and (14f) are all satisfied. According to Lemma 2, it follows that

$$f_{3,n}\left(p_n^{r*}, p_n^{BS*}, \theta_n^{*}\right) = \lambda_{n,0}^{*} \leq f_{6,n}\left(p_n^{r*}\right). \tag{68}$$

Thus, $\sum_{n=0}^{N-1} f_{6,n}\left(p_n^{r*}\right) \geq \lambda_0$ is obtained when (14f) and (68) are combined.

APPENDIX G
THE CONCAVE PROPERTY OF $f_{2,n}\left(p_n^r\right)$

Considering that $p_n^{BS} = a_n p_n^r + b_n$, which is given in (16), $f_{2,n}\left(p_n^r\right)$ can be expressed as

$$\begin{aligned} f_{2,n}\left(p_n^r\right) &= \ln\left(1+\Gamma_n^r\right) = \ln\left(1+\frac{a_0 p_n^r}{b_0 p_n^r + c_0}\right), \\ a_0 &= h_n^{rtr}, \\ b_0 &= h_n^{rcr} + a_n\left(h_n^{btr} + h_n^{bcr} + g_n^{br}\right), \\ c_0 &= b_n\left(h_n^{btr} + h_n^{bcr} + g_n^{br}\right) + \delta_n^2. \end{aligned} \tag{69}$$

The first and second derivative of $f_{2,n}\left(p_n^r\right)$ are given by

$$\begin{aligned} f_{2,n}'\left(p_n^r\right) &= \frac{a_0 c_0}{\left[\left(a_0+b_0\right)p_n^r + c_0\right]\left(b_0 p_n^r + c_0\right)} > 0, \\ f_{2,n}''\left(p_n^r\right) &= \frac{-a_0 c_0\left[2\left(a_0+b_0\right)b_0 p_n^r + \left(a_0+2b_0\right)c_0\right]}{\left[\left[\left(a_0+b_0\right)p_n^r + c_0\right]\left(b_0 p_n^r + c_0\right)\right]^2} \\ &< 0. \end{aligned} \tag{70}$$

For a given first derivative value of $f_{2,n}\left(p_n^r\right)$, i.e., $f_{2,n}'\left(p_n^r\right) = \mu_0$, p_n^r can be determined

$$\begin{aligned} p_n^r\left(\mu_0\right) &= \frac{-v + \sqrt{v^2 - 4\mu_0 w}}{2\mu_0}, \\ u &= \left(a_0+b_0\right)b_0, \\ v &= \left(a_0+2b_0\right)c_0, \\ w &= {c_0}^2 - \frac{a_0 c_0}{\mu_0}. \end{aligned} \tag{71}$$

REFERENCES

[1] C. Shi, S. Salous, F. Wang, and J. Zhou, "Low probability of intercept-based adaptive radar waveform optimization in signal-dependent clutter for joint radar and cellular communication systems," *EURASIP J. Adv. Signal Process.*, vol. 2016, no. 1, p. 111, Dec. 2016.

[2] C. Shi, F. Wang, M. Sellathurai, J. Zhou, and S. Salous, "Power minimization-based robust OFDM radar waveform design for radar and communication systems in coexistence," *IEEE Trans. Signal Process.*, vol. 66, no. 5, pp. 1316–1330, Mar. 2018.

[3] C. Shi, F. Wang, S. Salous, and J. Zhou, "Low probability of intercept-based optimal OFDM waveform design strategy for an integrated radar and communications system," *IEEE Access*, vol. 6, pp. 57689–57699, 2018.

[4] L. Chabod, R. Girard-Claudon, and E. Segura, "Taking benefit of radar resources in integrated RF sensor suites," in *Proc. Int. Radar Conf.*, Oct. 2014, pp. 1–5.

[5] P. Kumari, S. A. Vorobyov, and R. W. Heath, Jr., "Adaptive virtual waveform design for millimeter-wave joint communication-radar," 2019, *arXiv:1904.05516*. [Online]. Available: http://arxiv.org/abs/1904.05516

[6] S. H. Dokhanchi, M. R. B. Shankar, M. Alaee-Kerahroodi, T. Stifter, and B. Ottersten, "Adaptive waveform design for automotive joint radar-communications system," in *Proc. IEEE Int. Conf. Acoust., Speech Signal Process. (ICASSP)*, May 2019, pp. 4280–4284.

[7] G. C. Tavik, C. L. Hilterbrick, J. B. Evins, J. J. Alter, J. G. Crnkovich, J. W. de Graaf, W. Habicht, G. P. Hrin, S. A. Lessin, D. C. Wu, and S. M. Hagewood, "The advanced multifunction RF concept," *IEEE Trans. Microw. Theory Techn.*, vol. 53, no. 3, pp. 1009–1020, Mar. 2005.

[8] B. Li and A. P. Petropulu, "Joint transmit designs for coexistence of MIMO wireless communications and sparse sensing radars in clutter," *IEEE Trans. Aerosp. Electron. Syst.*, vol. 53, no. 6, pp. 2846–2864, Dec. 2017.

[9] F. Liu, C. Masouros, A. Li, T. Ratnarajah, and J. Zhou, "MIMO radar and cellular coexistence: A power-efficient approach enabled by interference exploitation," *IEEE Trans. Signal Process.*, vol. 66, no. 14, pp. 3681–3695, Jul. 2018.

[10] F. Liu, C. Masouros, A. Li, H. Sun, and L. Hanzo, "MU-MIMO communications with MIMO radar: From co-existence to joint transmission," *IEEE Trans. Wireless Commun.*, vol. 17, no. 4, pp. 2755–2770, Apr. 2018.

[11] F. Liu, C. Masouros, A. Li, and T. Ratnarajah, "Robust MIMO beamforming for cellular and radar coexistence," *IEEE Wireless Commun. Lett.*, vol. 6, no. 3, pp. 374–377, Jun. 2017.

[12] Y. Yang and R. Blum, "MIMO radar waveform design based on mutual information and minimum mean-square error estimation," *IEEE Trans. Aerosp. Electron. Syst.*, vol. 43, no. 1, pp. 330–343, Jan. 2007.

[13] M. Bica and V. Koivunen, "Generalized multicarrier radar: Models and performance," *IEEE Trans. Signal Process.*, vol. 64, no. 17, pp. 4389–4402, Sep. 2016.

[14] K.-W. Huang, M. Bica, U. Mitra, and V. Koivunen, "Radar waveform design in spectrum sharing environment: Coexistence and cognition," in *Proc. IEEE Radar Conf. (RadarCon)*, May 2015, pp. 1698–1703.

[15] M. Bica, K.-W. Huang, V. Koivunen, and U. Mitra, "Mutual information based radar waveform design for joint radar and cellular communication systems," in *Proc. IEEE Int. Conf. Acoust., Speech Signal Process. (ICASSP)*, Mar. 2016, pp. 3671–3675.

[16] M. Bica and V. Koivunen, "Multicarrier radar-communications waveform design for RF convergence and coexistence," in *Proc. IEEE Int. Conf. Acoust., Speech Signal Process. (ICASSP)*, May 2019, pp. 7780–7784.

[17] C. Shi, F. Wang, M. Sellathurai, and J. Zhou, "Non-cooperative game theoretic power allocation strategy for distributed multiple-radar architecture in a spectrum sharing environment," *IEEE Access*, vol. 6, pp. 17787–17800, 2018.

[18] B. Paul, A. R. Chiriyath, and D. W. Bliss, "Survey of RF communications and sensing convergence research," *IEEE Access*, vol. 5, pp. 252–270, 2017.

[19] D. W. Bliss, "Cooperative radar and communications signaling: The estimation and information theory odd couple," in *Proc. IEEE Radar Conf.*, May 2014, pp. 0050–0055.

[20] A. R. Chiriyath, B. Paul, and D. W. Bliss, "Radar-communications convergence: Coexistence, cooperation, and co-design," *IEEE Trans. Cognit. Commun. Netw.*, vol. 3, no. 1, pp. 1–12, Mar. 2017.

[21] A. R. Chiriyath, B. Paul, G. M. Jacyna, and D. W. Bliss, "Inner bounds on performance of radar and communications co-existence," *IEEE Trans. Signal Process.*, vol. 64, no. 2, pp. 464–474, Jan. 2016.

[22] A. R. Chiriyath, S. Ragi, H. D. Mittelmann, and D. W. Bliss, "Novel radar waveform optimization for a cooperative radar-communications system," *IEEE Trans. Aerosp. Electron. Syst.*, vol. 55, no. 3, pp. 1160–1173, Jun. 2019.
[23] Y. Liu, G. Liao, J. Xu, Z. Yang, and Y. Zhang, "Adaptive OFDM integrated radar and communications waveform design based on information theory," *IEEE Commun. Lett.*, vol. 21, no. 10, pp. 2174–2177, Oct. 2017.
[24] Y. Zhou, H. Zhou, F. Zhou, Y. Wu, and V. C. M. Leung, "Resource allocation for a wireless powered integrated radar and communication system," *IEEE Wireless Commun. Lett.*, vol. 8, no. 1, pp. 253–256, Feb. 2019.
[25] A. Daniyan, A. Aldowesh, Y. Gong, and S. Lambotharan, "Data association using game theory for multi-target tracking in passive bistatic radar," in *Proc. IEEE Radar Conf. (RadarConf)*, May 2017, pp. 0042–0046.
[26] A. Di Lallo, A. Farina, R. Fulcoli, A. Stile, L. Timmoneri, and D. Vigilante, "A real time test bed for 2D and 3D multi-radar tracking and data fusion with application to border control," in *Proc. CIE Int. Conf. Radar*, Oct. 2006, pp. 1–6.
[27] Y. J. A. Zhang, "Monotonic optimization in communication and networking systems," *Found. Trends Netw.*, vol. 7, no. 1, pp. 1–75, 2012.
[28] J. Yan, H. Liu, W. Pu, B. Jiu, Z. Liu, and Z. Bao, "Benefit analysis of data fusion for target tracking in multiple radar system," *IEEE Sensors J.*, vol. 16, no. 16, pp. 6359–6366, Aug. 2016.
[29] C. Shi, F. Wang, S. Salous, J. Zhou, and Z. Hu, "Nash bargaining game-theoretic framework for power control in distributed multiple-radar architecture underlying wireless communication system," *Entropy*, vol. 20, no. 4, p. 267, 2018.
[30] A. Turlapaty and Y. Jin, "A joint design of transmit waveforms for radar and communications systems in coexistence," in *Proc. IEEE Radar Conf.*, May 2014, pp. 0315–0319.
[31] M. R. Bell, "Information theory and radar waveform design," *IEEE Trans. Inf. Theory*, vol. 39, no. 5, pp. 1578–1597, Sep. 1993.
[32] D. Wu and R. Negi, "Effective capacity: A wireless link model for support of quality of service," *IEEE Trans. Wireless Commun.*, vol. 24, no. 5, pp. 630–643, May 2003.
[33] L. Musavian and Q. Ni, "Effective capacity maximization with statistical delay and effective energy efficiency requirements," *IEEE Trans. Wireless Commun.*, vol. 14, no. 7, pp. 3824–3835, Jul. 2015.
[34] L. Musavian and T. Le-Ngoc, "Energy-efficient power allocation over nakagami-*m* fading channels under delay-outage constraints," *IEEE Trans. Wireless Commun.*, vol. 13, no. 8, pp. 4081–4091, Apr. 2014.
[35] J. H. Bae, Y. S. Kim, N. Hur, and H. M. Kim, "Study on air-to-ground multipath channel and mobility influences in UAV based broadcasting," in *Proc. Int. Conf. Inf. Commun. Technol. Converg. (ICTC)*, Oct. 2018, pp. 1534–1538.
[36] Q. Feng, J. McGeehan, E. K. Tameh, and A. R. Nix, "Path loss models for Air-to-Ground radio channels in urban environments," in *Proc. IEEE 63rd Veh. Technol. Conf.*, vol. 6, May 2006, pp. 2901–2905.
[37] L. Wang, P. V. Brennan, H. Wang, and K.-K. Wong, "Minimax robust jamming techniques based on signal-to-interference-plus-noise ratio and mutual information criteria," *IET Commun.*, vol. 8, no. 10, pp. 1859–1867, Jul. 2014.
[38] Y. Yang and R. S. Blum, "Minimax robust MIMO radar waveform design," *IEEE J. Sel. Topics Signal Process.*, vol. 1, no. 1, pp. 147–155, Jun. 2007.

YUNFENG LIU received the B.S. degree from the Wuhan University of Technology (WUT), in 2014. He is currently pursuing the Ph.D. degree with the Key Laboratory of Universal Wireless Communications, Beijing University of Posts and Telecommunications, Beijing, China. His research interests include the wireless ad hoc/sensor networks, radio resource management of wireless personal area networks, and integrated radar and communication systems.

ZHIQING WEI (Member, IEEE) received the B.S. and Ph.D. degrees from the Beijing University of Posts and Telecommunications (BUPT), in 2010 and 2015, respectively. He is currently an Associate Professor with BUPT. His research interest includes the performance analysis and optimization of mobile ad hoc networks. He was a recipient of the Best Paper Award from the International Conference on Wireless Communications and Signal Processing (WCSP), in 2018.

CHENG YAN received the M.S. degree in signal and information processing from the Communication University of China (CUC), in 2014, and the Ph.D. degree from the Beijing University of Posts and Telecommunications, in 2018. He is currently with the North China Institute of Computing Technology. His research interests include machine to machine communications, 5G non-orthogonal multiple access technology, signal processing, mobile multimedia, and wireless communication.

ZHIYONG FENG (Senior Member, IEEE) received the B.S., M.S., and Ph.D. degrees from the Beijing University of Posts and Telecommunications, China. She is currently a Professor with BUPT. Her main research interests include the wireless network virtualization in the fifth-generation mobile networks (5G), spectrum sensing and dynamic spectrum management in cognitive wireless networks, universal signal detection and identification, and network information theory.

GORDON L. STÜBER (Fellow, IEEE) received the B.A.Sc. and Ph.D. degrees in electrical engineering from the University of Waterloo, Waterloo, ON, Canada, in 1982 and 1986, respectively. He was an IEEE Fellow, in 1999, for contributions to mobile radio and spread spectrum communications. He served as an Elected Member-at-Large for the IEEE Communications Society Board of Governors, from 2007 to 2009. He is currently an Elected Member of the IEEE Vehicular Technology Society Board of Governors, from 2001 to 2021, serving as the Awards Chair.